Stevin Laboratory
Faculty of Civil Engineering and Geosciences
Delft University of Technology

Report 25.5.10-16

December 2010

Shear Capacity of Concrete Beams without Shear Reinforcement under Sustained Loads

Literature Survey

Ir. R. Sarkhosh / Ir. J.A. den Uijl / Dr.ir. C.R. Braam /
Prof.dr.ir. J.C. Walraven

Mailing address:
Delft University of Technology (TU-Delft)
Faculty of Civil Engineering and Geosciences
Concrete Structures Group
Stevin Laboratory II
Stevinweg 1
2628 CN Delft
The Netherlands

Table of Contents

CONTENTS page

Introduction 3
Chapter 1: Short-Term Shear Failure 4
1.1. Shear flexure capacity 7
1.2. Shear tension capacity 13
1.3. Loads near to supports 14
Chapter 2: Shear transfer mechanisms and influencing parameters 17
2.1. Shear transfer in compression zone 18
2.2. Dowel action 18
2.3. Aggregate interlock 19
2.4. Concrete strength 20
2.5. Shear span to depth ratio 20
2.6. Axial force 21
2.7. Influence of bond 22
2.8. Design equations for shear capacity 22
2.8.1. Historical development 22
2.8.2. Code Review 25
2.9. Fracture mechanics 29
Chapter 3: Time Dependency 36
3.1. Development of Strength and modulus of elasticity with time 36
3.2. Strength and deformation under sustained high loads 37
3.3. Definitions of Time-Dependent Deformations 39
Chapter 4: Modelling 46
4.1. Rough-crack model of Baźant and Gambarova 47
4.2. Two-phase model of Walraven 48
4.3. Model of Wittmann and Zaitsev 50
4.4. Dugdale model 52
4.5. FE Model of Petersson, Hillerberg and Modéer 52
4.6. Model of Zhou and Hillerborg 55
References 58

Introduction

Concrete is a multiphase granular material consisting of aggregate particles of various sizes and irregular shape, embedded in hardened cement paste. The physicochemical processes during the hardening of the cement cause air voids, micro cracks and interfacial bond micro cracks. As a consequence of this heterogeneous structure, concrete displays a non-linear and time-dependent deformation response under sustained loading.

A challenging topic was and still is the failure behaviour of concrete beams without shear reinforcement. The behaviour of cracked reinforced concrete panels can now be satisfactorily predicted for monotonic short-term shear loading conditions. In spite of substantial experimental and theoretical efforts in the past, the shear transfer mechanism in concrete in the case of sustained shear loads is not well known.

When a concrete beam is under sustained high loads, a flexural cracking pattern appears along the span. Here, various shear-carrying mechanisms may be developed by a beam, e.g. aggregate-interlock and dowel action. These mechanisms induce tensile stresses in concrete near the crack tip and at the level of the reinforcement. Once the tensile strength of the concrete in these regions is reached, the existing flexural cracks progress in a diagonal direction or new ones are created. The development of the critical shear crack, however, does not necessarily imply the collapse of the member but in case of sustained high loads, the crack width and therefore the crack length will be increased.

The aim of this research is to predict the time-dependent mechanical behaviour of cracked concrete beams subjected to sustained shear loads. The results should enable the designer to quantify the failure load (ULS) and deformations and the propagation of the cracks (SLS) of beams under sustained shear loads.

Chapter 1: Short-Term Shear Failure

The behaviour of a slender beam subject to a gradually increasing load and its failure in flexure is well known. The first cracks will appear long before the failure load is reached. The cracks are narrow and unimportant provided the reinforcing steel tensile strain is less than about 0.1 percent in a crack. Due to bond, the steel and concrete attain the same mean strain so that with a value of 0.1 percent the stress in steel would be about 210 MPa (E_s = 210 GPa). Under further loading, the cracks increase both in width and length indicating that the area of the compressive zone decreases. In the concrete, the increase of the internal lever arm contributes to carrying the increased load. This effect is combined with the gradual increase of internal forces (steel tensile force and concrete compressive force). This effect is especially visible when the stress in the steel reaches and exceeds the yield point stress. The force resisted by the steel and concrete now remains almost constant. An increase in the load is to be resisted by an increase of the internal lever arm only. As a result, strains increase considerably.

When the bending process is continued, the strain in the outer fibres of the compressive zone increases rapidly. This increase is mainly due to the decrease in the area of the compressive zone as a result of cracking due to the increase in the load. Thus the strain in the compressive zone eventually reaches the failure strain of concrete and destruction of the compressive zone brings about the flexural failure of the beam.

There is no disagreement on what constitutes flexural failure, but there is a strong disagreement on what shear failure is, even as far as the meaning of that term itself is concerned. Some researchers think, for instance, that failure of the bond between steel and concrete represents a typical shear failure, while others consider it as a third type of failure (after flexural failure and shear failure). Because shear failure appears to be an unsuitable term for a failure in which shear has little or no influence and also because a diagonal crack is a visible feature of all failures which are not flexural failures, some research workers, e.g. Kani [18], classify these two main groups of failures of reinforced concrete beams under ‘flexural failure’ and ‘diagonal failure’. Of course, there is still the possibility that more than one type of diagonal failure exists.

Most researchers state that there are three principle methods in which a reinforced concrete beam can fail in shear. The first type of shear failure is a web crushing failure. For a web crushing failure, the concrete compressive strength is exceeded and the web crushes typically at the top flange of an I-shaped section near the applied load. For a web crushing failure, the cracking is initiated in the web and then extends out in both directions. The second type of shear failure is called a flexural shear failure. For this type of failure, the initial cracks form due to flexure at a 90-degree angle with respect to the longitudinal axis of the beam ($\tau = 0$ at the outer fibres). As the externally applied load increases, shear forces and principal tensile stresses dominate the flexural effects causing the cracks to change direction (close to a 45 degree angle from the longitudinal axis) and continue until the principal stresses produce enough dilation of the crack to cause failure. The third type of failure occurs in the discontinuity regions of the beam where plane sections don’t remain plane due to the load being applied so close to the support. Typical failure mechanisms occur due to arching action between the applied load and the support. The Eurocode 2, the AASHTO LRFD and the ACI 318-08 design codes account for these three types of failure.

Shear failure of reinforced concrete beams without web reinforcement is usually caused by inclined diagonal tension cracking (Fig. 1). Once the diagonal tension cracks develop in the web of the beam, the beam without web reinforcement becomes unstable. ASCE-ACI Committee 426 [1] reported that for cracked beams the shear resistance is developed by several shear transfer mechanisms (Fig. 2). First, the intact uncracked concrete in the compression zone is capable of transferring the shear force (V_{cc}). However, in a slender beam, the contribution of the shear force at the compression zone does not account for the major part of the total shear resistance.

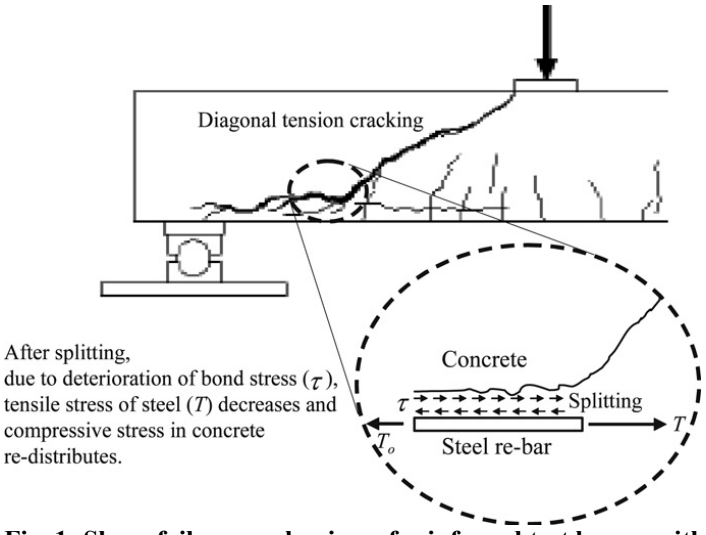

Fig. 1: Shear failure mechanism of reinforced test beams without shear reinforcement [23]

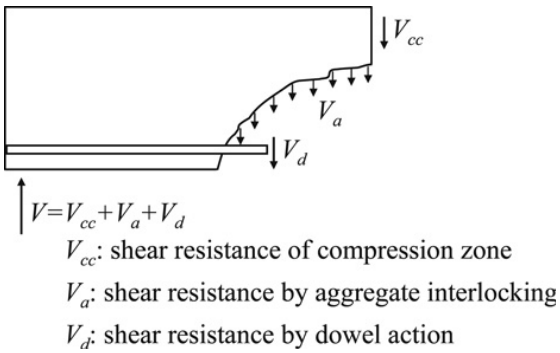

Fig. 2: Several components of shear resistance

According to test results by Walraven [3], a large amount of the shear force is transferred along the cracked surface via aggregate interlocking (V_a). Usually, this shear transfer mechanism is known to be dependent on the aggregate size [2], the compressive strength of the concrete [7] and the fracture mode of concrete (in the aggregate or the concrete transition zone; Loov and Peng [8]). The contribution of the dowel action of the longitudinal reinforcement (V_d) to shear strength has been researched by Vintzeleou and Tassios [9]. The first researches on shear failure were conducted by Teller and Sutherland [10] and Timoshenko et al. [11].

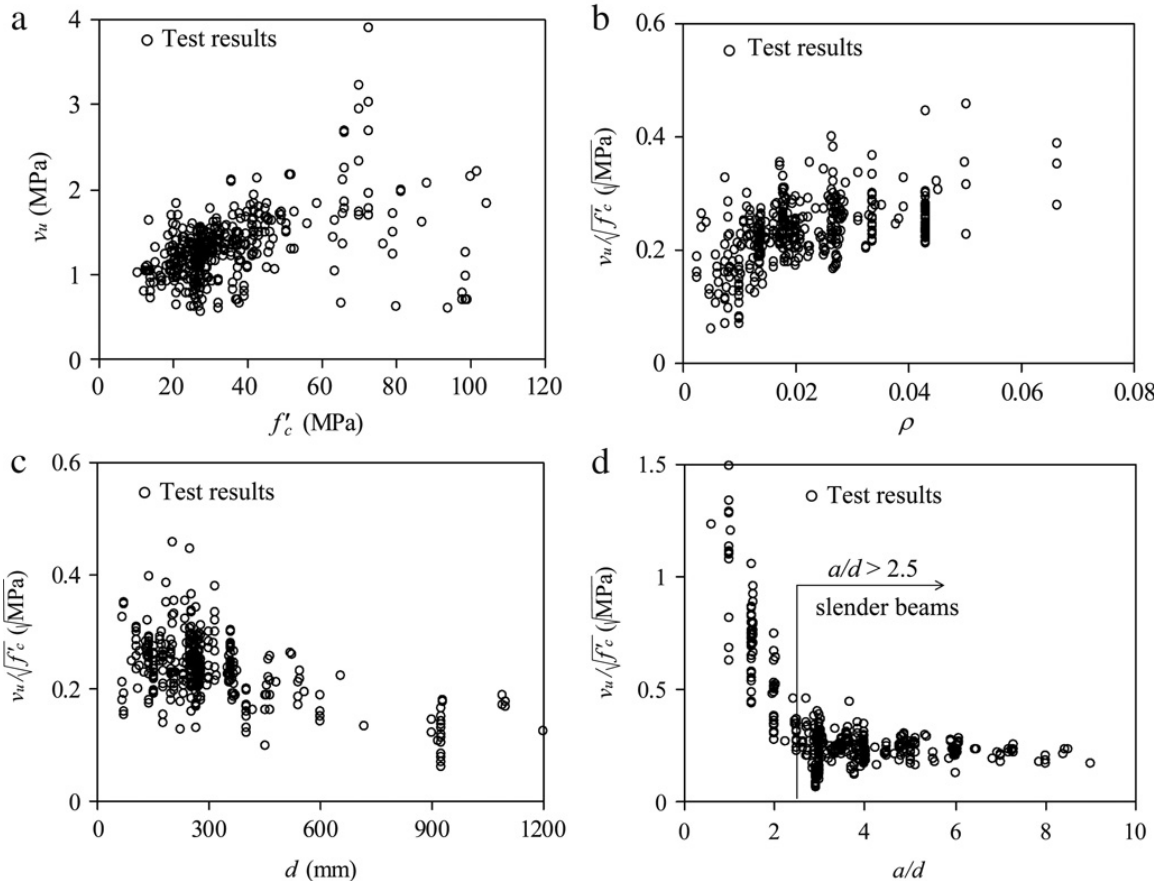

Fig. 3: Variations of shear strength of beams according to primary design parameters: (a) compressive strength of concrete; (b) reinforcement ratio; (c) effective depth; and (d) shear span to depth ratio [33]

When shear deformations occur in cracked concrete, the tension reinforcement designed to resist the bending moment, is subjected to a certain amount of shear stress. However, it is known that in case of concrete beams without shear reinforcement, dowel action of this reinforcement becomes insignificant because the maximum shear developed in the longitudinal reinforcement is limited by the tensile strength of the concrete cover supporting this reinforcement (ASCE-ACI Committee 445 [12]). According to existing test results, the shear resisting mechanism is affected mainly by concrete strength, tension reinforcement ratio, effective depth, and shear span to depth ratio as shown in Fig. 3.

Talbot [13] suggested that the shear strength of slender beams varies with the amount of tension reinforcement ratio as well as the compressive strength of the concrete (Fig. 3 (a) and (b)). The experimental studies by Kani [14] and Shioya et al. [16] showed that the shear strength of concrete beams decreases as the size of the beam increases, in spite of keeping cross-section geometry, material properties, and reinforcement ratios of the beams constant (Fig. 3 (c)). Bažant [17] showed that to satisfy the condition of energy balance, the size effect must be addressed in the evaluation of shear strengths of brittle materials like concrete. Kani [18] showed that for deep beams and relatively short beams (a/d <2.5), the shear resistance may be affected by the shear span to depth ratio (a/d) because part of the applied shear force may be transmitted directly to the supports by arch action (compressive struts) of the concrete. Slender beams were therefore defined to be those beams with a/d > 2.5 as shown in Fig. 3(d).

However, the shear failure mechanism of reinforced concrete beams without web reinforcement is a complex phenomenon that is difficult to analyze accurately. The shear

failure may be suddenly developed by various local failures including crushing of concrete in the web or at the supports or the loaded area, anchorage failure (Zararis [22]), and splitting between the longitudinal reinforcement and the concrete in the cracked section (Tureyen and Frosch [23]). The shear strength may be also affected by various parameters (which are considered as minor parameters) such as maximum aggregate size, diameter of longitudinal bars, and spacing between the cracks [24].

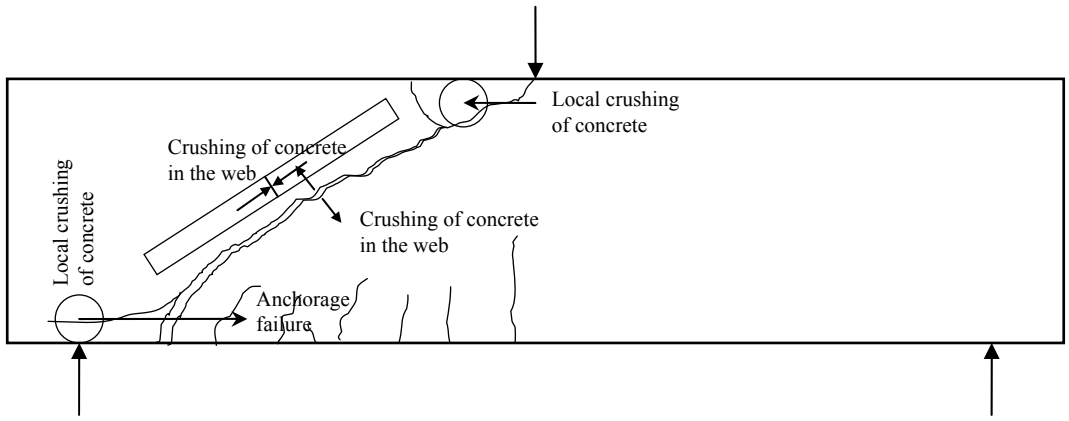

Fig. 4: Schematic view of the shear failure of concrete beam

1.1. Shear flexure capacity

Most shear failures occur in the region of the member cracked in flexure. It is necessary to make a distinction between shear flexure and shear tension. The recommendations for the determination of the shear flexure capacity of members not reinforced in shear are given chapter 6.2.2 of prENV 1992-1-1 [28].

$$V_{Rd1} = [\tau_{Rd} \cdot k\,(1.2 + 40\,\rho_l) + 0.15\sigma_{cp}] \cdot b_w \cdot d \qquad (1)$$

where

τ_{Rd} basic shear strength, which follows from $\tau_{Rd} = 0.25 f_{ctk,0.05}/\gamma_c$.
k factor allowing for the size effect, equal to $k = 1.6 - d$ (m) > 1
ρ_l flexural tensile reinforcement ratio, $A_s/b_w\,d < 0.02$
σ_{cp} design axial stress (if any) = N_{Ed}/A_c
b_w minimum web section

This equation has been derived in the following way. The basic equation adopted, which was believed to take appropriate account of the most important influencing factors like concrete strength, longitudinal reinforcement ratio and cross-sectional height was

$$V_u = C \cdot k\,(100 \cdot \rho_l \cdot f_c)^{1/3} \cdot b_w \cdot d \qquad (2)$$

where

k = size factor = $1 + (200/d)^{1/2}$
ρ_l = longitudinal reinforcement ratio
f_c = concrete cylinder strength (N/mm^2)
C = coefficient to be determined

A selection was made of a representative number of shear tests, considering a parameter variation as wide as possible and as well as possible distributed within practical limits. This was already done by König and Fischer [47]. An overview of the test parameters is given in Fig. 5. Then for every test result the optimum value C was determined. If the distribution is normal, Fig. 6, a lower bound value for C was determined according to the level 2 method described by Taerwe [64] with the equation:

$$C_{\text{lower bond}} = C_{\text{mean}} \cdot (1 - \alpha \cdot \beta \cdot v) \tag{3}$$

where

α sensitivity factor, equal to 0.8 for the case of one dominating variable (concrete strength)

β reliability index, taken equal to 3.8 according to [Eurocode, Basis of Structural design, Draft version 2001]

v standard deviation

If the distribution turns out to be log-normal, Fig. 6, the equation is

$$C_{\text{lower bond}} = C_{\text{mean}} \cdot \exp(\alpha \cdot \beta \cdot v - 0.5\, v^2) \tag{4}$$

In these equations a reliability index $\beta = 3.8$ means a probability of occurrence of 0.0072%. König and Fischer [47] carried out this procedure for 176 shear tests. As a result of their analysis they found that a coefficient $C = 0.12$ would be a good lower bound. In Fig. 7 it is shown that the prediction accuracy of this equation is substantially better than that of the old EC-1992-1-1 formula (Eq. 1).

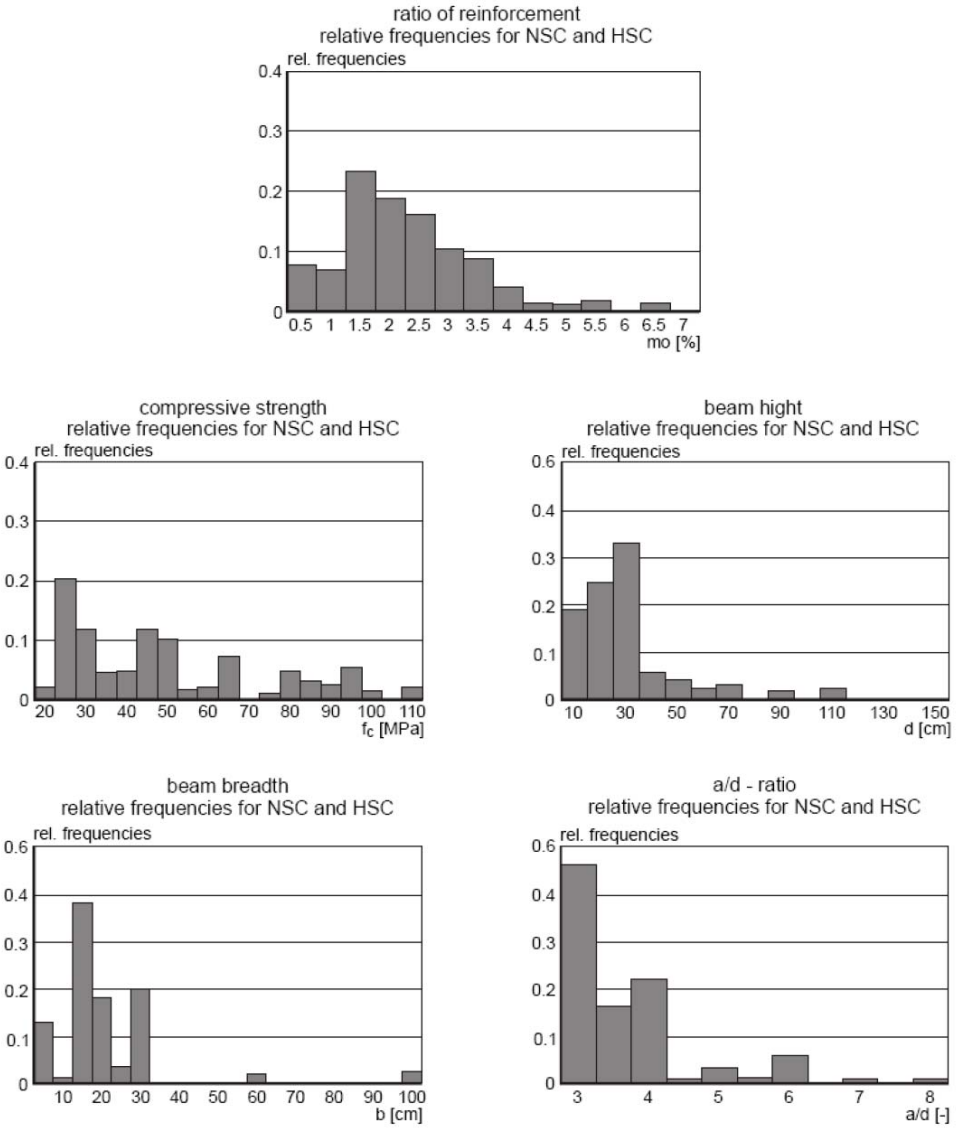

Fig. 5: Relative frequency of parameters in test data bank used by König and Fischer [47] in order to find a reliable lower bound equation for the shear capacity of members without shear reinforcement

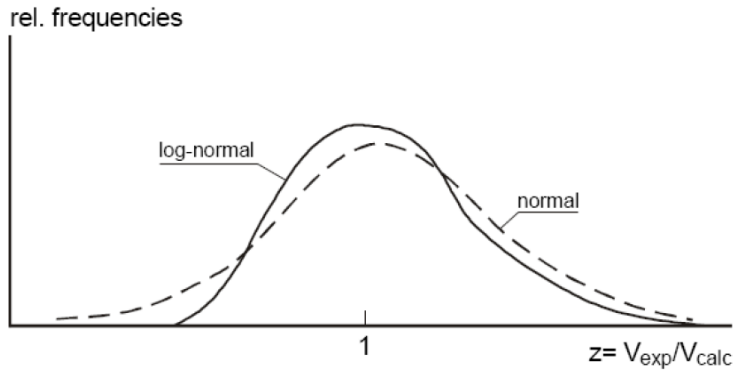

Fig. 6: Normal and log-normal distribution

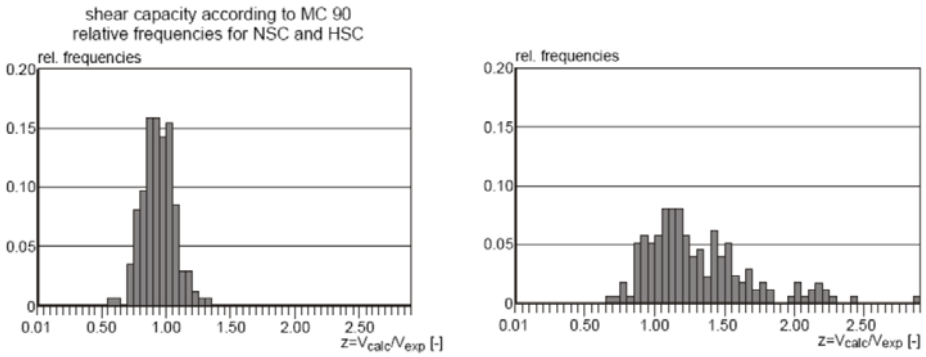

Fig. 7: Left) Shear capacity according to Eq. 2 (MC 90): relative frequency for NSC and HSC. Right) Shear capacity according to Eq. 1 (ENV 1992-1-1): relative frequency for NSC and HSC [47]

It was however argued, that the equation

$$V_{Rd,c} = 0.12\, k\, (100\, \rho_l \cdot f_{ck})^{1/3} \cdot b_w \cdot d \qquad (5)$$

has two disadvantages; The first is that it does not distinguish between persistent & transient loading combinations and accidental loading combinations, for which different safety levels apply (prEN 1992- 1-1:2001 chapter 2.4.1.4 gives $\gamma_c = 1.5$ for persistent and transient and $\gamma_c = 1.2$ for accidental situations). Therefore the equation was modified by introducing the concrete safety factor explicitly.

$$V_{Rd,c} = (0.18/\gamma_c)\, k\, (100\, \rho_l \cdot f_{ck})^{1/3} \cdot b_w \cdot d \qquad (6)$$

The second is that the shear capacity goes to 0 when $\rho_l = 0$. Furthermore it was wished to have a simple conservative value for $V_{Rd,c}$ for a first check of the bearing capacity. In many countries simple formulations have been used on the basis of

$$V_{Rd,c} = C \cdot f_{ctd} \cdot b_w \cdot d \qquad (7)$$

where f_{ctd} is the design tensile strength of the concrete and C is a coefficient. Practice in the various countries however is quite different because C varies in the range from 0.3 to 0.75.

Considering the value of C it should be noted that this equation is a simplification of the rigorous one. To have general validity, even for rare but still possible cases, C should be based on the most unfavourable combination of parameters. That means that the governing case is a slab with a large cross-sectional depth d and a low longitudinal reinforcement ratio. In his paper "Basic facts concerning shear failure", Kani [20] showed that shear failures are unlikely to occur for longitudinal reinforcement ratio's smaller than 0.6%. However, his "shear valley" was based on beams with a cross-sectional effective depth of only $d = 270$ mm. For larger depths the critical value of ρ_0 decreases. Therefore a number of shear failures reported by Aster, Koch [2], Walraven [4] and Mathey, Watstein [5] have been selected with large d and small ρ_0 values, see Table 1.

The most unfavourable values for C are 0,34, found for Aster and Koch's tests Nr.11 and 16, with $d = 500$ and 750 mm and $\rho_0 = 0{,}46$ and 0,42% respectively.

Table 1: Determination of *C* on the basis of selected tests

Beam	d [mm]	b [mm]	a/d	ρ_0 [%]	f_{cm} [MPa]	$V_{u,exp}$ [MPa]	f_{ck} [MPa]	f_{ctm} [MPa]	f_{ctk} [MPa]	C
Aster, Koch (1974) [2]										
2	250	1000	3.7	0.64	27.5	0.88	19.5	2.17	1.52	0.58
3	250	1000	3.7	0.91	27.6	0.90	19.6	2.18	1.52	0.59
11	500	1000	3.7	0.46	28.4	0.53	20.4	2.24	1.56	0.34
12	500	1000	3.7	0.65	27.6	0.66	19.6	2.18	1.52	0.43
16	750	1000	3.7	0.42	28.3	0.53	20.3	2.23	1.56	0.34
Walraven (1978) [4]										
A1	125	200	3	0.83	27.5	1.19	19.5	2.17	1.52	0.78
A2	420	200	3	0.74	27.5	0.84	19.5	2.17	1.52	0.55
A3	720	200	3	0.79	27.5	0.70	19.5	2.17	1.52	0.46
Mathey, Watstein (1963) [5]										
Via24	403	203	3.8	0.47	26.3	0.67	18.3	2.09	1.46	0.46
Via25	403	203	3.8	0.47	25.8	0.61	17.8	2.05	1.43	0.43

So, with some rounding off a value $C = 0.35$ would be appropriate for the simplified design equation. In prEN 1992-1-1:2001 a value 0.40 is used. An argument might be that the utmost part of the practical cases consists of slabs with smaller depths, subjected to uniform loading, where the maximum shear force does not coincide with the maximum moment, and the reinforcement ratio's are small enough to ensure failure by bending. The specific case of a slab spanning in one direction, with a high cross-section, a critically low reinforcement ratio and a line load just at the most critical position from the support would then have a slightly lower safety. On the other hand formula's should always be safe enough to take account of any possible (not likely) case, which would be an argument in favour of the use of 0.35.

Some questions may be raised with regard to the definition of b_w being "the smallest width of the cross-section in the tensile area". Tests on tapered cross-sections showed that there is certainly an influence of the definition of the web width, as shown in Fig. 8, left (tests by Leung, Chew and Regan [6]). Fig. 8, right, shows that a definition of b_w as the average width of the beam would be appropriate for this case.

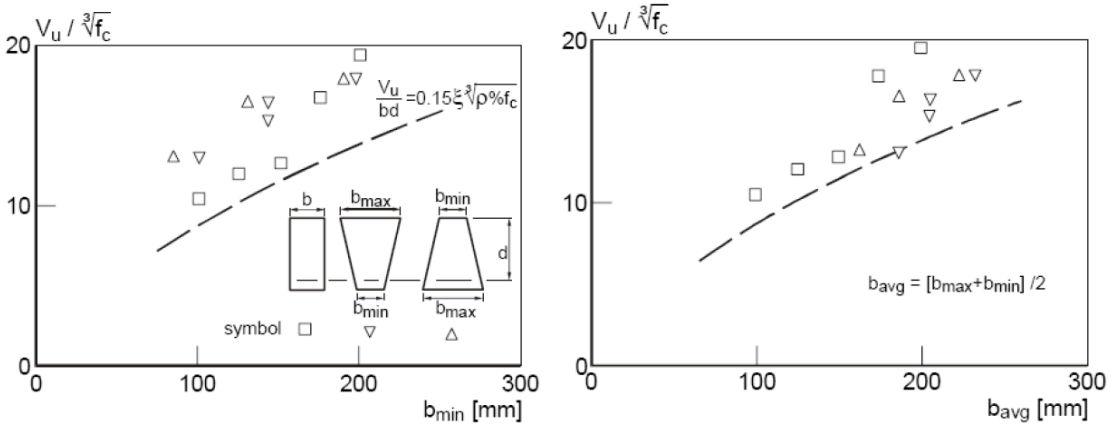

Fig. 8: Shear resistance of beams with tapered cross-section (Leung, Chew and Regan [6])

In a more recent publication (Regan [46]) the author opts for a definition of $b_w = \frac{2}{3}b_{min} + \frac{1}{3}b_{max}$, but admits at the same time that the available evidence is rather scarce. A possible compromise could be to define b_w as the average width of the part of the cross-section in tension, with a maximum of 1.25 of the minimum width.

The equations in prEN 1991-1-1:2001 contain as well a term $0.15\sigma_{cp}$ regarding the influence of an axial force on the shear capacity, for instance by prestressing. Basically the influence of prestressing can be taken into account as proposed by Hedman & Losberg [34]. It was argued that, with regard to the behaviour in shear, a prestressed beam can be regarded as a reinforced beam after the decompression moment has been reached. On the basis of this argument the shear resistance was formulated as

$$V_{Rd,c} = V_c + V_p \tag{8}$$

where V_c is the shear resistance of a similar non-prestressed beam and V_p is the contribution of the prestressing force to the shear capacity, which can be formulated as $V_p = M_0/a$, where M_0 is the decompression moment and a is the distance from the load to the support, Fig. 9.

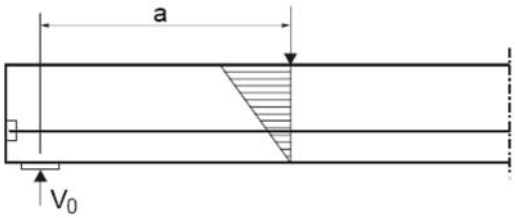

Fig. 9: Calculation of contribution *V*p from prestressing to the shear resistance according to Hedman and Losberg [34]

However, this method works well for the evaluation of laboratory tests but is less suitable for real members mostly subjected to uniformly distributed loading. A solution is to replace M_0/a by $M_0/(M_x/V_x)$, where M_x and V_x are the bending moment and the shear force in the section considered. However, this would complicate the shear design because then V_p would be different in any cross-section. Another disadvantage is that V_p would go to infinity in a moment inflexion point, where $M_x = 0$.

It can simply be derived that for a rectangular cross-section with a width b, a height h and an eccentricity of the prestressing force e_p, the contribution V_p to the shear resistance is

$$V_p = F_p\,(1/6 + e_p/h)/(a/h) \tag{9}$$

Assuming $d = 0.85h$ this would result in;

$$V_p = 1.18\,F_p\,(1/6 + e_p/h)/(a/d) \tag{10}$$

In most tests on shear critical beams the ratio e_p/h is about 0.35. With a/d varying between 2.5 and 4.0, like in most shear tests, this would mean that V_p would vary between $0.15\sigma_{cp}\cdot b\cdot d$ and $0.25\sigma_{cp}\cdot b\cdot d$. When evaluating test results it is therefore not amazing that the coefficient 0.15 turns out to be a safe lower bound in shear critical regions. Nielsen [49] compared the shear equation in ENV 1992-1-1 which gives about the same results as Eq. 6.2a in prEN 1992-1-1:2001 for moderate concrete strengths, with 287 test results and found that it was at the safe side.

The effect of longitudinal compression should, of course, not be mixed up with the effect of the cable curvature, which exerts a favourable transverse load on the member. This effect, known as the load balancing effect, is introduced as a load (load balancing principle).

For axial tension in prEN 1992-1-1 the same formula is used, with a different sign for $0.15\sigma_{cp}$, so that an axial tensile force gives rise to a slight reduction of the shear capacity. It should be noted that in continuous beams there is tension in both top and bottom and excessive curtailment at sections of contra flexure may lead to diagonal cracking and shear failure in such a region. This was the main cause of failure in an actual structure (Hognestadt and Elstner [50]). If a structural member is well designed for axial tension the shear capacity of the members is hardly reduced. This was for instance shown by Regan [52] and [53], who carried out a systematic investigation into the effect of an axial tensile force on the shear capacity of both members unreinforced and reinforced for shear. Tests have been carried out according to the principle shown in Fig. 10. Beams with a rectangular cross-section were provided with nibs, enabling the transmission of an axial tensile force in the middle part. The axial tensile force varied between 0 and 130 kN. The force could be applied in two ways: before subjecting the member to transverse loading, or in proportion to the transverse loading. In both cases the shear capacity was hardly influenced, although the member sometimes showed wide open cracks across the total cross section in the moment inflexion region.

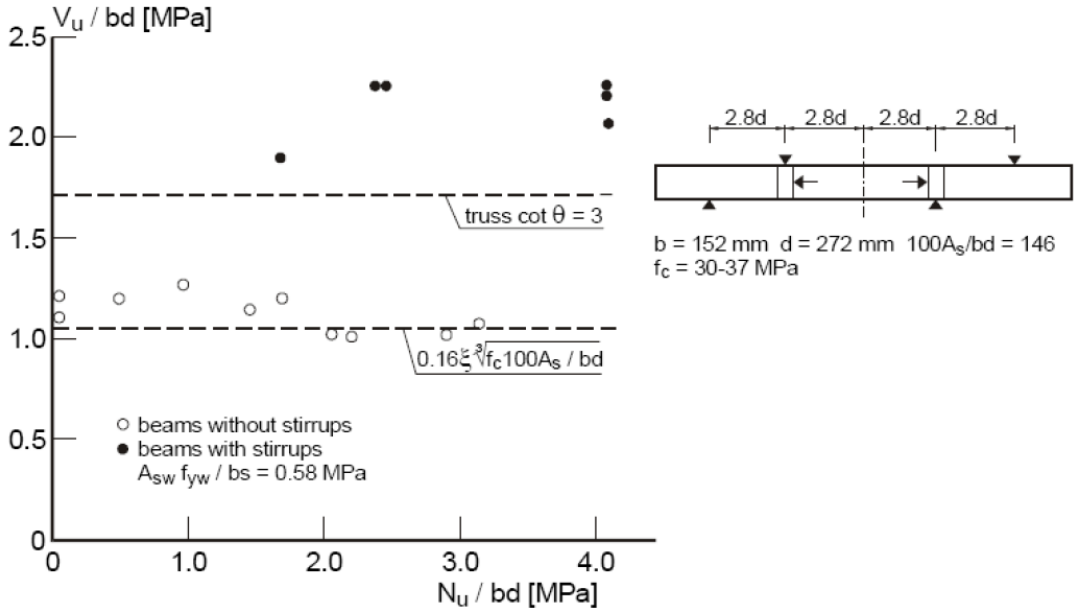

Fig. 10: Results of tests on beams subjected to axial tension, bending and shear, and failing in shear [53]

1.2. Shear tension capacity

In special cases, like for instance when pretensioned strands are used in members with reduced web widths, such as in prestressed hollow core slabs, shear tension failures can occur, Fig. 11.

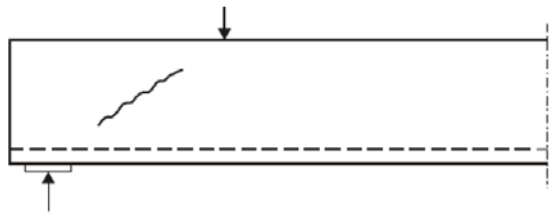

Fig. 11: Shear tension failure

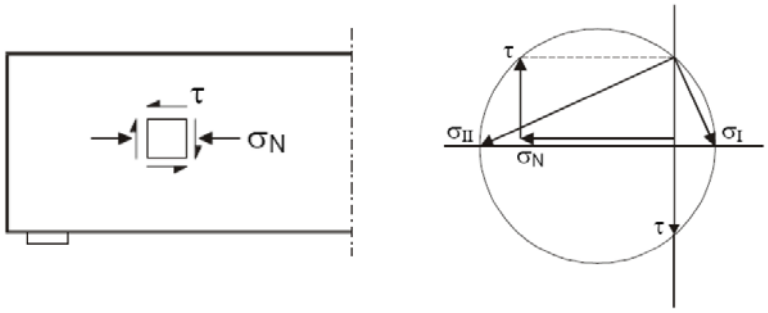

Fig. 12: Calculation of shear tension capacity with Mohr's circle

In this case failure occurs due to the fact that the principal tensile stress in the web reaches the tensile strength of the concrete in the region uncracked in flexure. The principal tensile strength in the web calculated using Mohr's circle, Fig. 12, is equal to

$$\sigma_I = -\tfrac{1}{2}\sigma_N + \sqrt{(\tau^2 + \tfrac{1}{4}\sigma_N^2)} \tag{11}$$

Substituting $\tau = V_{Rd,ct} \cdot S/b_w I$ and $\sigma_N = \alpha_1 \cdot \sigma_{cp}$ in above equation, the code's expression EC-2, Eq. 6.3

$$V_{Rd,ct} = \frac{I \cdot b_w}{S}\sqrt{(f_{ctd})^2 + \alpha_1 \sigma_{cp} f_{ctd}} \tag{12}$$

is obtained.

1.3. Loads near to supports

The Eq. (5) or in prENV 1992-1-1:2001 the Equation 6.2.a, is extended with a factor ($2d/x$) in order to cope with the increased shear capacity in the case of loads applied near to supports. According to this formulation, at a distance $0.5d < x < 2d$ the shear capacity may be increased to

$$V_{Rd,ct} = 0.12\ k\ (100\ \rho\ f_{ck})^{1/3}(2d/x) b_w\ d \tag{13}$$

This may need some explanation, since it might be argued that loads near to supports may be treated with the rules given in EC-2, 2001 version, chapter 6.5 "Design of discontinuity regions with strut and tie models". However, there are many arguments in favour of the formulation according to Eq. 13;

- According to the formulations for the strut and tie model the capacity of the concrete struts only depends on the strength of the concrete, see e.g. Fig. 13. Consequently, the maximum capacity is a function of the concrete strength, the inclination of the strut and the width of the support area.

It can easily be seen that this is a very simplified representation of reality, since the capacity of such a member results to be independent of the slenderness ratio a/d, which is known to have a strong influence. Furthermore short members are prone to significant size effects. It was shown (Walraven and Lehwalter [79]), that the size effect in short members is the same for short and slender members, so that here also the factor $k = 1 + \sqrt{(200/d)}$ applies.

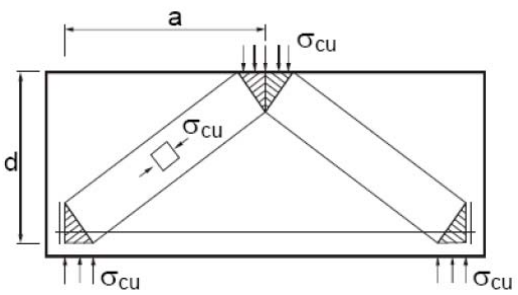

Fig. 13: Bearing capacity of short member according to strut and tie model with defined maximum concrete stress in the struts

Walraven and Lehwalter carried out tests on short members with various sizes, a/d ratio's and support widths, and compared the equivalent maximum stress in the concrete struts, Fig. 14. The dotted plane is valid for a maximum stress $0.6f_c$. It is seen that for lower a/d ratio's the capacity is considerably higher than the one obtained with the strut and tie model. It is seen furthermore that the limit $0.55f_c$ for struts with transverse tension is appropriate for $a/d < 2.0$, members with depths until 1 m and a support width (k) up to about $0.20d$.

For a number of practical members, like in the case of corbels and pile caps, it is important to reduce the size as much as possible. A more accurate formulation than the strut and tie model is therefore useful in those cases.

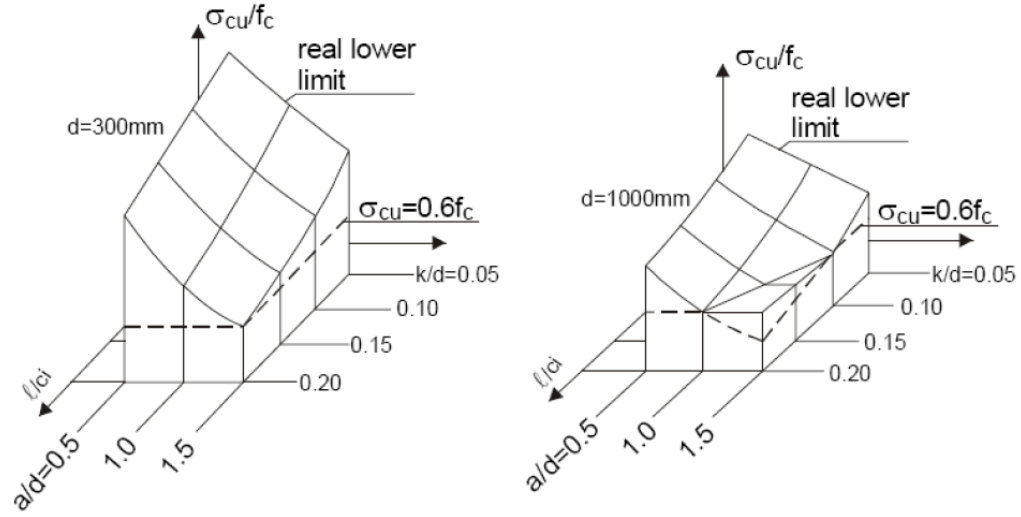

Fig. 14: Maximum stress in concrete struts as calculated on the basis of test results [79]

- Another case is shown in Fig. 15. It is a part of a foundation caisson in the Storebaelt Bridge, with a slab of about 1 m and wall distances of about 5 m. A substantial part of the counter pressure of the soil is transmitted directly to the walls, so that the governing shear load is small. Without a provision like the one given in Eq. 13, unnecessary shear reinforcement would be required.

By introducing the distance x and determining the shear capacity in every cross section, also combinations of loads (like two concentrated loads, or a uniformly distributed load and a concentrated load) can be handled. An important question is whether the multiplication factor should be ($3d/a$, $2.5d/a$ or $2d/a$). Regan [32], on the basis of the analysis of many experiments, concluded that [30]:

a. For simply supported beams subjected to concentrated loads a factor (2.5d/a) is appropriate. This is confirmed in Fig. 16:
b. For continuous beams with concentrated loads even (3d/a) gives safe results.
c. For simply supported beams subjected to distributed loading only (2d/a) gives safe results.

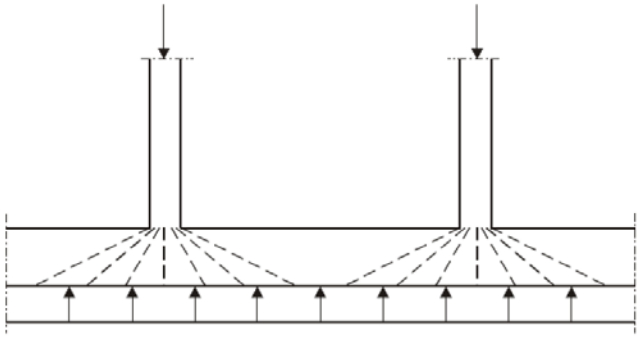

Fig. 15: Foundation slab in Storebaelt caisson

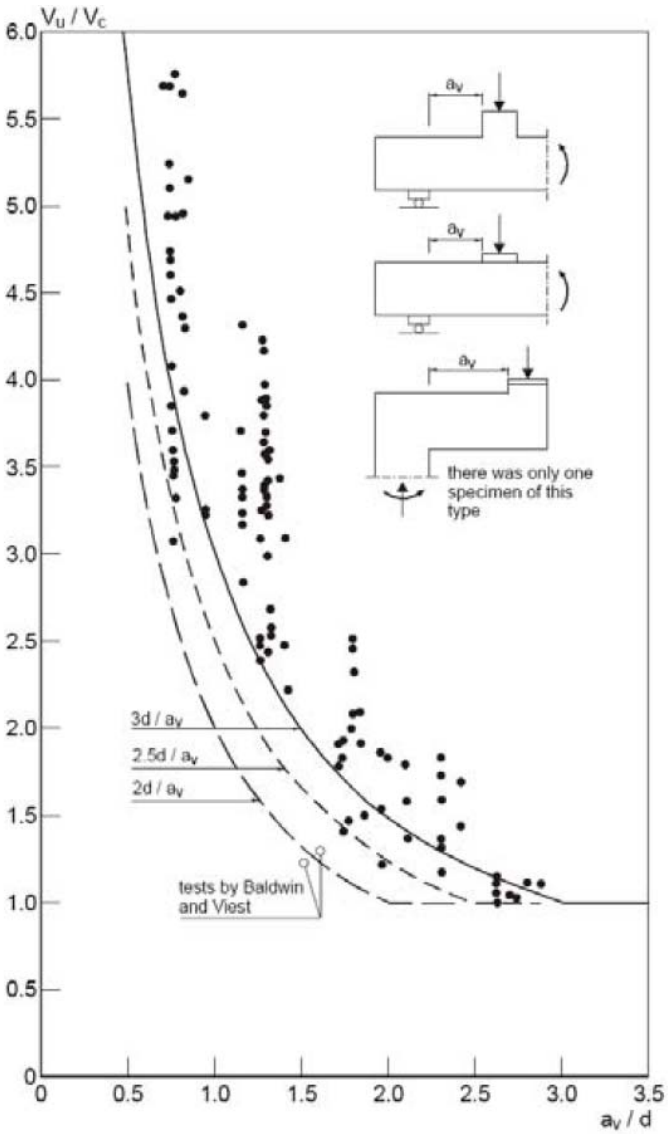

Fig. 16: Results of tests on simply supported beams without shear reinforcement subjected to concentrated loads [32]

Chapter 2: Shear transfer mechanisms and influencing parameters

Shear transfer mechanisms in concrete beams are complex and difficult to identify clearly due to the complex stress redistributions that occur after cracking. Shear transfer mechanisms have been shown to be influenced by various factors. Fig. 17 describes the basic mechanisms of shear transfer in accordance with the findings of the state-of-the-art reports by joint ASCE-ACI Committee 426 [1] and joint ASCE-ACI Committee 445 [12], which are now generally accepted in the research community. The important shear transfer mechanisms are shear in the uncracked compression zone of the beam, interface shear transfer due to aggregate interlock or surface roughness of the cracks, dowel action of the longitudinal reinforcement, and residual tensile stresses across the crack. However, it should be noted that different researchers impose different levels of relative importance to these basic mechanisms of shear transfer.

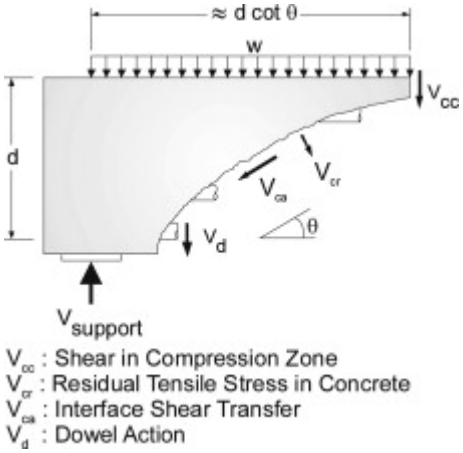

Fig. 17: Shear transfer/actions contributing to shear resistance

Several parameters have been identified as having a significant influence on the contributions of the shear resistance mechanisms and, as a result, on the shear capacity. The influences of the most dominant mechanisms are known as concrete strength, size effect, span to depth ratio, longitudinal reinforcement ratio, axial force. There are other less dominant influencing parameters such as support conditions, loading points, etc. All these parameters are included in three important factors;

a) shear transfer in the compression zone (area of concrete in compression)
b) dowel action of longitudinal reinforcing bars crossing the crack in concrete
c) aggregate interlock across the crack face

It is assumed that the shear resistance, V_{Rd} is derived from a shear capacity (stress), τ_c acting uniformly over the effective area of the section. Rafla [45] presented an empirical formula for the shear capacity or average shear stress τ_c of a section;

$$\tau_c = 0.29\ \alpha_u\ \alpha_h\ (f_{cm})^{1/2}\ (\rho)^{1/3}$$

where,

$\alpha_u = 0.795 + 0.293\ (3.5 - a/d)^{2.5}$ for $2.0 \leq a/d \leq 3.5$

$\alpha_h = 1/(d/100)^{1/4}$

f_{cm} is the cube strength of concrete [MPa]
a is shear span [mm]
d is effective depth [mm]
and ρ is ratio of tensile reinforcement in %.

2.1. Shear transfer in compression zone

The uncracked portion of a cracked concrete beam is subjected to both compressive and shearing stresses. Thus, this portion of the concrete beam contributes to shear resistance. The magnitude of the resistance depends on the depth of the uncracked concrete.

Fig. 17 indicates that uncracked concrete (i.e. the compressive zone of the beam cross section) is subjected not only to an axial compressive force (due to bending moment) but also to the shear force. Although the magnitude of the nominal shear stress (i.e. the ratio of the shear force to the area of the compressive zone of the cross section) exceeds (in the region where the depth of the uncracked concrete is small) the concrete shear capacity (as defined in current codes), the mechanism of shear resistance enables uncracked concrete to sustain the applied shear force. In compliance with this mechanism, the presence of biaxial stress conditions (in a localized region of the compressive zone where the depth is small) delays the development of tensile stresses (caused by the shear force). Therefore, the value of the shear force required to cause failure of the compressive zone becomes larger than the force expected to cause failure in compliance with the concepts underlying current design methods [66]. For less slender beams, at the location of the maximum moment, much of the shear is resisted in the compression zone, particularly after significant yielding of the longitudinal reinforcement [67]. However, because the depth of the compression zone is relatively small for slender members without axial compression, most of the codes neglect the effect of the compression zone on the shear capacity of the beam.

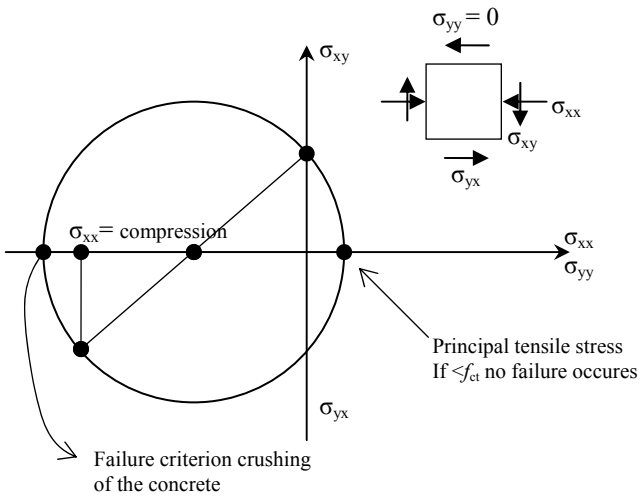

Fig. 18: Failure criterion "crushing of the concrete" shown on Mohr's circle

2.2. Dowel action

The phenomenon of dowel action as a shear transfer mechanism across cracks has long been recognized as an important component of the overall shear resistance capacity of reinforced concrete beams. The dowel action of reinforcing bars can play an important role if other

contributions to shear transfer are relatively small as in the case of a beam with a small amount of web reinforcement or in case of a post-peak stage of the loading process. It may contribute significantly to the post-peak resistance and hence contribute to the shear ductility of concrete members. In experimental tests, the shear force transferred by the dowel action is quite difficult to measure because it is embedded with other shear transfer components. Even in finite element analysis, the mechanism of the dowel action is complicated. To analyze the details of dowel action, the steel bars need to be individually modelled by finite elements and a very fine mesh has to be used for the concrete to account for the influence of, for instance the concrete cover. As a result, the number of elements required would be very large. Furthermore, such individual modelling of the steel bars and concrete is not compatible with the common practice of modelling the concrete and the steel together (perfect bond) in the analysis of reinforced concrete structures.

2.3. Aggregate interlock

Aggregate interlock is highly dependent on the crack opening and the shearing and frictional properties of the aggregate particles along the crack surface. The shear load transfer through aggregate interlock further depends on aggregate type and size, crack tortuosity, concrete strength and stiffness, size of the cracked cross-sectional area, boundary conditions, load magnitude and load repetitions. Leonhardt [38] presents the relation of aggregate size to the size of the beam and explains that the aggregate interlock mainly depends on this relation and the amount of large size aggregates. Based on his research, the interlock of usual aggregates up to 30 mm size is more effective in beams with small depth (about 200 mm), than in deeper beams. Many researchers have found that the shear strength of beams without shear reinforcement decreases considerably with increasing depth, if the aggregate size is kept constant [39].

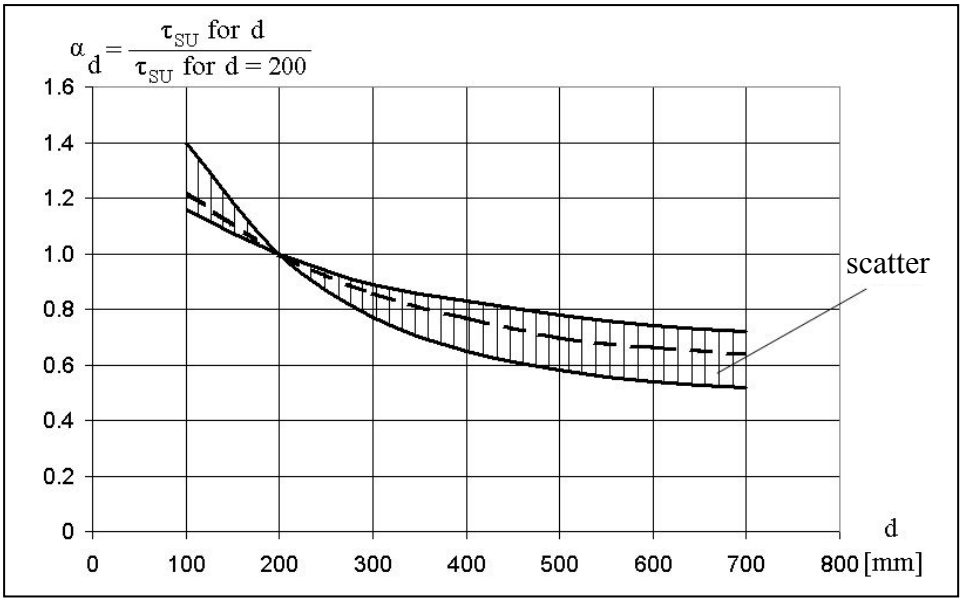

Fig. 19: Influence of absolute depth on shear strength of beams without shear reinforcement [39]

2.4. Concrete strength

The shear strength increases as the concrete strength increases. In many design codes, the shear strength of a member is usually taken as directly proportional to $f_c^{1/3}$ to $f_c^{1/2}$, which indicates that the concrete ultimate tensile strength is being used as the governing parameter. However in case of allowable stresses, Kani [21] reported a totally opposite conclusion. Based on results derived from his experimental tests, the influence of the concrete strength (f_c) on the shear strength of R.C. beams is so small that, within a tolerance of ±10%, this parameter can be omitted from the strength analysis and in formulas for allowable stresses.

The shear strength of members without stirrups, traditionally correlated to the square root of the concrete compressive strength (after the works of Moody et al. [82]), is strongly dependent on the critical shear crack width and on shear crack plane roughness. The critical shear crack theory reflects this dependency as;

$$\frac{V_R}{bd} = \sqrt{f_c} \cdot f\,(w, d_g) \tag{14}$$

where f_c is the concrete compressive strength, w is the critical shear crack width, and d_g is the maximum aggregate size [83].

2.5. Shear span to depth ratio

There is one more important parameter for the shear strength of slabs or rectangular beams; this is the moment/shear-ratio in relation to the depth $M/V_s\,d$ which for concentrated loads is equals to a/d, see Fig. 20, (the max M of the span has to be related to max V at support). It was found that the bending moment at shear failure is lowest for $a/d \approx 3$. It increases steeply for $a/d < 3$, concentrated loads are closer to the bearing. It increases also for loads having larger distances than $a/d = 3$ and it reaches the full bending failure moment at $a/d \approx 7$ for high percentages of reinforcement.

Kani [20] called this diagram the "valley of diagonal failure" and presented it for different reinforcement ratios (Fig. 21). He found that the depth of the valley decreases with decreasing percentages of reinforcement and practically disappears for percentages below 0.6%, referring to reinforcing steel with a yield strength of 400 MPa.

Many empirical formulas for calculating the shear strength include the a/d ratio to account for the influence of this parameter. This phenomenon is quite significant in members with the a/d ratio less than about 2.5, because a portion of shear may be transmitted directly to the support by an inclined strut. For those deep members, therefore, it is more appropriate to use strut-and-tie models than sectional design approaches.

For the same magnitude of loading, as the longitudinal reinforcement ratio decreases, flexural stresses and strains increase (reduction of relative concrete compression zone height x/d). Thus, the crack widths increase and the shear strength is reduced. Further, as the longitudinal reinforcement ratio decreases, dowel action also decreases.

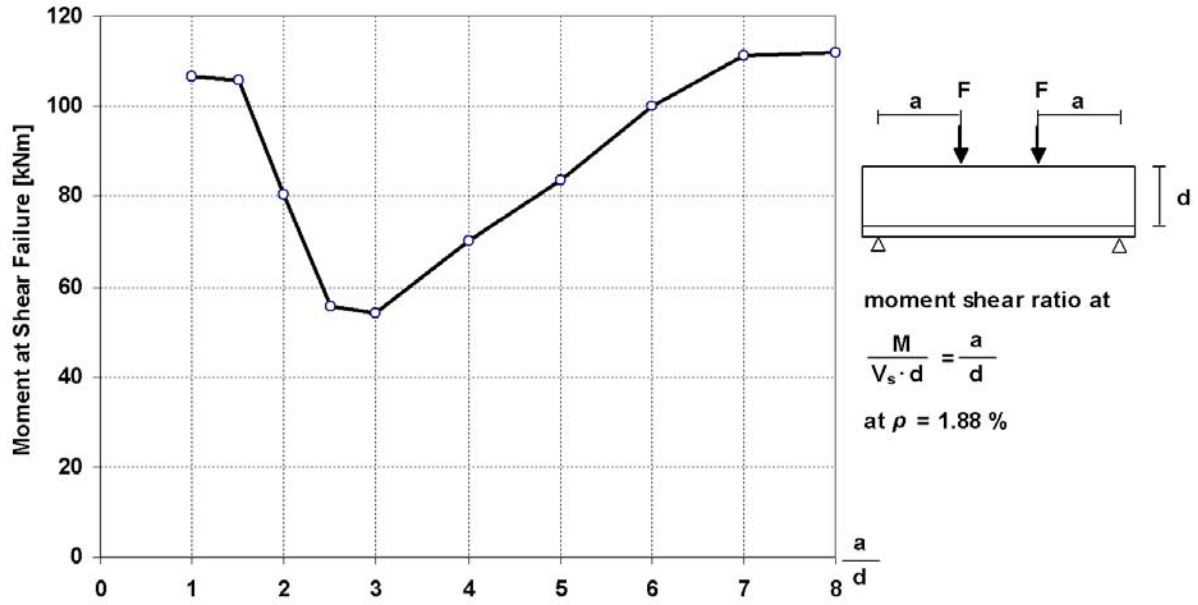

Fig. 20: Influence of load distance from support on shear strength for ρ=1.88 % [20]

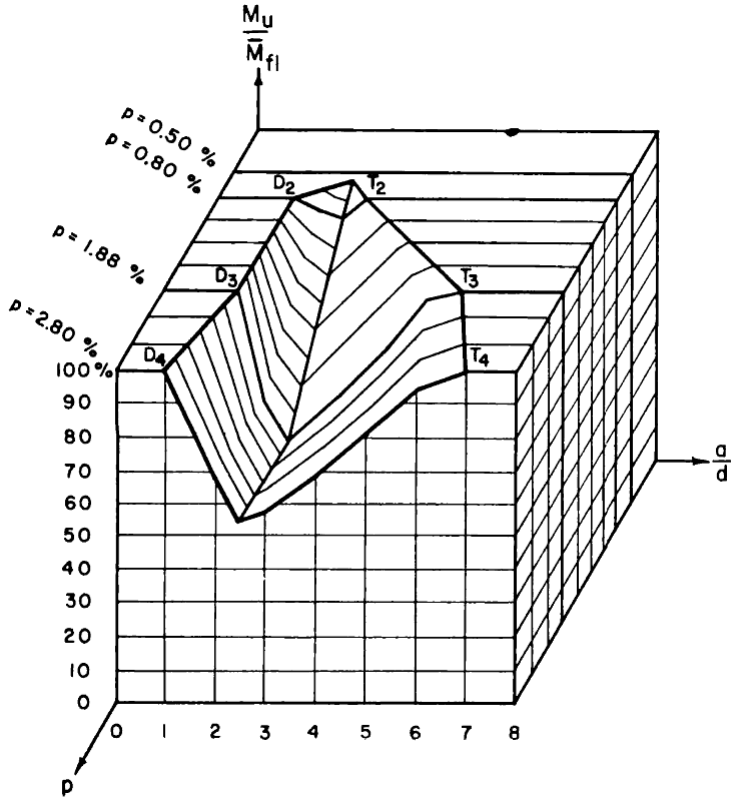

Fig. 21: Kani's shear failure valley. Shear strength dependent on a/d and ρ_L = reinforcement ratio [20]

2.6. Axial force

When the members are subjected to axial tension, the shear strength of such members decreases. By contrast, axial compression increases the depth of the uncracked compression zone, decreases the width of the shear cracks, and thus the compression zone and the interface shear transfer is increased. The equations in prEN 1991-1-1:2001 contain as well a term

$0.15\sigma_{cp}$ regarding the influence of an axial force on the shear capacity, for instance by prestressing. The influence of axial force is briefly discussed in section 1.1.

2.7. Influence of bond

A well-known fact about bond refers to the spacing of cracks. Good bond creates closely spaced cracks, while poor or nonexistent bond results in only a few cracks or no cracks at all in the end section of the beam, i.e., in the part where a shear force exists. That means that under conditions of poor bond the crack distances Δx will be relatively large, see Fig. 22. Considering the distance between parallel cracks as one concrete tooth, the load-carrying capacity of concrete tooth at failure is given by

$$M_{CR} = (7/8)\,(f_t'/6) \cdot (\Delta x/s) \cdot b \cdot a \cdot d \qquad (15)$$

where, s is vertical crack length

For two beams, identical in every respect except bond resistance, the one with poor bond, and therefore large Δx, will have a higher load-carrying capacity than the beam with good bond [18]. The surprising result is: *the better the bond, the lower the diagonal load-carrying capacity*.

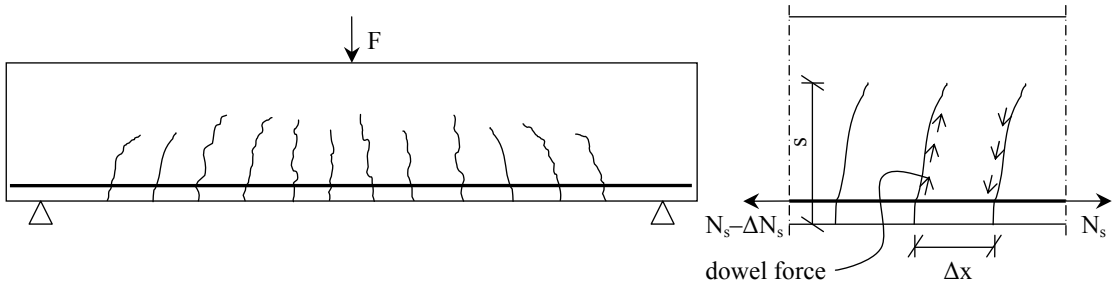

Fig. 22: Concrete teeth in cracked beam

The influence of bond on shear capacity of R.C. beams is investigated by Leonhardt and Walther [54]. Their test series consisted of eight beams, all having the same cross section (190 × 320 mm), same percentage of longitudinal reinforcement (1.90 percent), same concrete (21 MPa) and same span (2000 mm). Half of them were reinforced with deformed bars, the other half with very smooth bars. To investigate the influence of bar diameter on load-carrying capacity, two arrangements of steel at the same steel percentage were used. In all cases, poorer bond resulted in an increase of the load-carrying capacity as Eq. (15) predicted. The beams with poor bond carried at least 31 percent more load than the corresponding beams with deformed bars. The beams with poor bond reached their flexural failure, while the beams with deformed bars stayed far below their full flexural capacity.

2.8. Design equations for shear capacity

2.8.1. Historical development

Prior to cracking, the maximum shear stress at the web can be calculated by using the traditional theory for homogenous, elastic and uncracked beams, developed by Russian engineer Jourawski in 1856 [18]:

$$\tau = \frac{VQ}{I\,b} \tag{16}$$

where I is the moment of inertia of the cross section, Q is the first moment about the centroidal axis of the part of the cross sectional area lying farther from the centroidal axis than the point where the shear stresses are being calculated, and b is the width of the member where the stresses are being calculated.

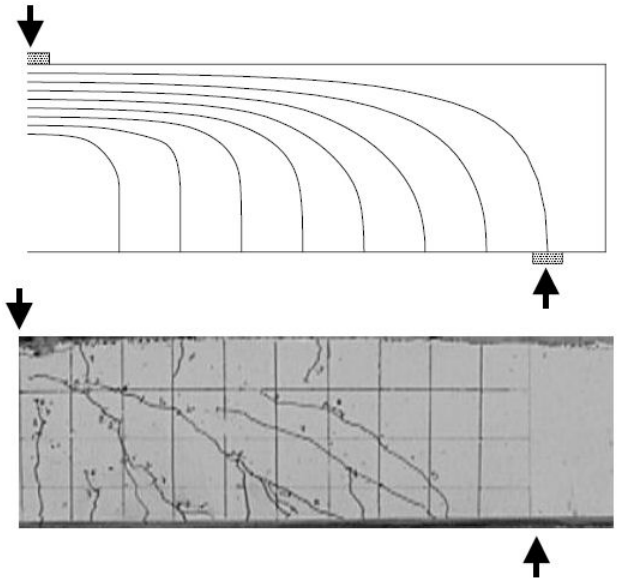

Fig. 23: Principal compressive stress trajectories in an uncracked beam and photograph of a cracked reinforced concrete beam

Fig. 23 shows the principal compressive stress trajectories in an uncracked beam and a photograph of a cracked reinforced concrete beam. Although there is similarity between the planes of maximum principal tensile stress and the cracking pattern, they are by no means exactly alike. The flexural cracking which precedes the inclined cracking, disrupts the elastic stress filed to such an extent that inclined cracking occurs at a principal tensile stress, based on the uncracked section, of roughly a third of the tensile strength of the concrete [37].

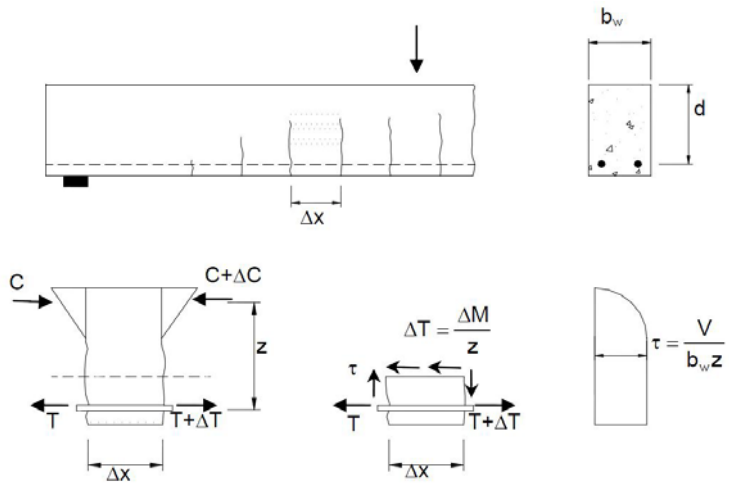

Fig. 24: shear stress distribution in a reinforced concrete beam with flexural cracks

In 1902 Mörsch derived the shear stress distribution for a reinforced concrete beam containing flexural cracks. Mörsch predicted that the shear stress would reach its maximum value at the

neutral axis and would then remain constant from the neutral axis down to the flexural steel (Fig. 24). The value of this maximum shear stress would be;

$$\tau = \frac{V}{b_w z} \tag{17}$$

Where b_w is the web width and z is the flexural lever arm.

Mörsch recognised that this was a simplification, as some of the transverse force could be resisted by an inclination in the main compression, which would cause the ribs of the concrete between flexural cracks to bend, producing dowel forces in the main steel.

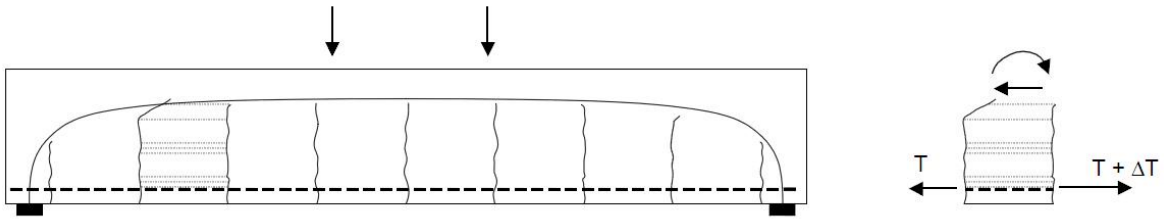

Fig. 25: Kani's comb model for cracked beam subjected to shear

In 1964, Kani attempted a more realistic approach by addressing the problem of the bending the "teeth of the concrete" between flexural cracks [19]. The concrete between two adjacent flexural cracks was considered to be analogous to a tooth in a comb (Fig. 25). The concrete teeth were assumed to be free cantilevers fixed in the compression zone of the beams and loaded by the horizontal shear from bonded reinforcement. Although this theory did not cover most of the shear transfer mechanisms, it was probably the start of more rational approaches.

Fenwick and Paulay [36], working with "tooth model", pointed out the significance of the forces transferred across cracks in normal beams by crack friction. Taylor [40], also evaluating Kani's model, found that for normal test beams the components of shear resistance were: compression zone shear (20-40%), crack friction (35-50%) and dowel action (15-25%).

Hamadi and Regan [41] based on extensive experimental work on interface shear, published an analysis of a tooth model. It was assumed that the cracks were vertical and that their spacing was equal to half the effective depth of a particular beam.

Empirically derived equations have been very important in the development of procedures used for designing members without transverse reinforcement. The simplest lower-bound average shear stress at diagonal cracking is given in an ACI expression:

$$\frac{V_c}{bd} = \tau = \frac{\sqrt{f_c}}{6} \tag{18}$$

This equation is a reasonable lower bound for smaller slender beams that are not subjected to axial load and have at least 1% longitudinal reinforcement [42]. However, it may be unconservative for lowly-reinforced members and high-strength concrete members.

The CEB-FIP Model Code [57] suggests a more sophisticated empirical formula and adds an extra term to account for the size effect.

$$\frac{V_c}{bd} = 0.12\left(1+\sqrt{\frac{200}{d}}\right)\left(\frac{3d}{a}\right)^{1/3}\left(100\rho_s f_{ck}\right)^{1/3} - 0.15\sigma_{cd} \quad (19)$$

where, σ_{cd} equals to N_d/A_c, N_d is the factored axial force that includes the prestress (tensile positive) force and A_c is the cross sectional area of the concrete.

It should be noted that the formula implicitly includes the concrete safety factor. To disregard this factor, the constant 0.12 should be replaced by 0.15.

The MC-90 equation takes the influences of compression force as a factor. However, members without shear reinforcement subjected to large axial compression and shear may fail in a very brittle manner at the first instance of diagonal cracking [67]. Other different fracture mechanics models have been proposed to account for the fact that a peak tensile stress is near the tip of a crack and a reduced tensile stress (softening) is located in the crack zone. This approach offers a possible explanation for the size effect in shear. Two well-known models are the Fictitious Crack Model [43] and Crack Band Model [44].

The Modified Compression Field Theory (MCFT) is a general model for the load-deformation behaviour of two dimensional cracked reinforced concrete subjected to shear [7]. The MCFT is formulated in terms of average stresses and requires an additional check to ensure that the loads resisted by the average stresses can be transmitted across the crack. For members without transverse reinforcement, the local stresses at a crack always control the capacity of the member, and the average stress calculation is used only for estimating the inclination of the critical diagonal crack.

2.8.2. Code Review

Most analytical models, such as the modified compression field theory [9], strut and tie [25], and truss models [26], include important semi-empirical expressions such as the expressions for concrete softening in the stress-strain relationship [27] or the concrete cracking angle for truss models [26]. In design practice, complex theoretical models, are usually abandoned and replaced by simple design methods such as those used by European code EC2 [28], the American code ACI 318-05 [29] and the Canadian code CSA- 04 [31] listed in Table 2.

Table 2. Existing design codes for beams without web reinforcement

Investigator	Shear strength models (MPa)
EC2 [28]	$\upsilon_{Rd,c} = 0.18k\,(100\,\rho\, f_{ck})^{1/3}$, f_c in MPa $k = 1 + (200/d)^{1/2} \le 2.0$, d in mm $\rho \le 0.02$
ACI 318-05 [29]	$\upsilon_c = 0.158\,(f_c)^{1/2} + 17.2\,\rho_w\, V_u d/M_u$, f_c in MPa or $\upsilon_c = 0.167\,(f_c)^{1/2}$, f_c in MPa V_u = shear force, M_u = flexural moment
CSA [31]	$\upsilon_c = \lambda_t\,\beta\,(f_c)^{1/2}\,(d_v/d)$ λ_t = factor to account for low-density concrete (= 1) β=[0.4/(1+1500ε_x)].[1300/(1000+S_{ze})] ε_x=[M_f/d_v+V_f]/(2E_sA_s)$\ge$ 0,$\varepsilon_x \le 0.003$ V_f = shear force, M_f = flexural moment S_{ze}=35S_z/(15+d_a) $\ge$ 0.85S_z Sz = d_v [= max (0.9d , 0.72h)] f_c' in MPa. d and d_v in mm

	d_a = maximum aggregate size (mm)
AASHTO LRFD 2000	$V_a = \beta (f_c)^{1/2} b_v d_v$ The values β and d_v depends on the equivalent crack spacing parameter and b_v is the web thickness

I. Eurocode 2

There are two possibilities to look at the formula in EC2. The first possibility, one can say a more academic view, is to take into account the history of the formula. This means to interpret the formula as it is meant. The second possibility is to interpret the formula as it is, without consideration of its history [47]. Each possibility leads to different equations which enable the comparison with test results. In the present case, both possibilities are investigated

Interpretation with consideration of history

A short report is given about the history of the design equation to get a formula for the shear capacity which enables the comparison with the results. In CEB-Bulletin 126 [48] the factor c in the below equation was determined with the help of a regression analysis.

$$v = c \cdot (1 + 50 \cdot \rho_1) \cdot (f_{cm})^{1/2} \tag{20}$$

This analysis provided a mean value of

$$c_m = 0.09 \tag{21}$$

which gives a 5%-fractile value of

$$c_{5\%} = 0.068 \tag{22}$$

For an assumption for the coefficient of variation of $\delta_c = 0.15$. Then the relation below for the concrete tensile strength was used.

$$f_{ctm} = 0.375 (f_{cm})^{1/2} \tag{23}$$

With an assumption for the coefficient of variation of the tensile strength of $\delta_{fct} = 0.15$ the characteristic value followed:

$$f_{ctk} = 0.375 (1 - 1.645 \cdot 0.15) \cdot (f_{cm})^{1/2} = 0.282 (f_{cm})^{1/2} \tag{24}$$

When substituting this result in equation (20) yielded the characteristic value for the shear capacity:

$$v_k = c_{5\%} \cdot (1 + 50 \rho_1) \cdot (f_{cm})^{1/2} = 0.068 (1 + 50 \rho_1) \cdot f_{ctk} / 0.282 \approx 0.25 (1 + 50 \rho_1) \cdot f_{ctk} \tag{25}$$

To consider the influence of the effective depth d, the size effect factor k was introduced, so that the final equation became

$$v_k = 0.25 \cdot k \cdot (1 + 50 \rho_1) \cdot f_{ctk} \tag{26}$$

To obtain a formula based on the compressive strength of concrete, EC2 states the following two equations;

$f_{ctk;0.05} = 0.7 f_{ctm}$
$f_{ctm} = 0.3 (f_{ck})^{2/3}$ (27)

By dividing through the safety factor $\gamma_c = 1.5$ and changing of the term in brackets (by the way no explanation could be found for this changing) the design value for the shear capacity becomes

$$v_k = 0.25 \cdot 0.7 \cdot 0.3 \cdot (f_{ck})^{2/3} \cdot k \cdot (1.2 + 40\,\rho_1) / \gamma_c = 0.035 \cdot k \cdot (1.2 + 40\,\rho_1) \cdot (f_{ck})^{2/3} \quad (28)$$

The characteristic value for the shear capacity respectively (γ_c =1.0) becomes

$$v_k = 0.0525 \cdot (1.2 + 40\,\rho_1) \cdot (f_{ck})^{2/3} \quad (29)$$

Within the scope of model uncertainties equation (29) has to be judged. For that purpose it is necessary to convert this equation to get a comparison with test results. This is possible by replacing equation (22) with equation (21) and setting γ_c =1.0. All other relations are only equivalent replacements for $(f_{cm})^{1/2}$ and can be maintained. So for the comparison of test results the following relation has to be used.

$$v_m = 0.09 \cdot 0.7 \cdot 0.3 \cdot (f_{ck})^{2/3} \cdot k \cdot (1.2 + 40\,\rho_1) / 0.282 = 0.067 \cdot k \cdot (1.2 + 40\,\rho_1) \cdot (f_{ck})^{2/3} \quad (30)$$

$(f_{ck})^{2/3}$ implies no safety elements because it is an equivalent substitute for the expression $(f_{cm})^{1/2}$. Thus the real value for f_{ck} has to be inserted. Distinction has to be made between two cases;

I. The way of determining of compressive strength of concrete is known
   If all information about the determining of f_c is available (number of samples and individual results), f_{ck} can be determined by common statistical methods.
II. The way of determining the compressive strength of concrete in unknown
   If no information is available a useful assumption has to be made. In all probability the given values for f_c in literature are mean values. So the relation $f_{ck} = f_{cm} - 8$ N/mm^2 (EC2, table 4.3) can be used for normal strength concrete up to 60 MPa.

<u>Interpretation without consideration of history</u>

This procedure is shown because some authors prefer to come from the following equation;

$$v_{Rd1} = \tau_{rd} \cdot k \cdot (1.2 + 40\,\rho_1) \quad (31)$$

The shear resistance of concrete members without shear reinforcement in EC2-April 2002 final draft, is given as;

$$V_{Rd,c} = [(0.18/\gamma_c) \cdot k \cdot (100\,\rho_l \cdot f_{ck})^{1/3} + 0.15\,\sigma_{cp}]\, b_w \cdot d \quad (32)$$

With a minimum of

$$V_{Rd,min} = [(0.035) \cdot k^{3/2} \cdot f_{ck}^{1/2}]\, b_w \cdot d \quad (33)$$

where,
$\gamma_c = 1.5$
f_{ck} is in MPa and $f_{ck} \leq 100$ MPa.

$\sigma_{cp} = N_{sd} / A_c$
N_{sd} is the design value of the normal force (external)
A_c is the concrete area ($b \cdot h$)
and factor k is equal to 1.0 for sections where more than 50% of the tensile reinforcement is curtailed and is equal to $1.6 - d \geq 1.0$ in other cases.

II. Modelcode 1990 (MC 1990)

The formula for the design value of the shear capacity in MC90 was derived from

$$v = c \cdot \xi \cdot (100 \cdot \rho \cdot f_c)^{1/3} \tag{34}$$

III. Dutch Code NEN 6720

The shear capacity of concrete beams can be calculated from:

$$\tau_1 = 0.4 f_b k_\lambda k_h (\omega_o)^{1/3} > 0.4 f_b \tag{35}$$

where;
$k_\lambda = 12/g_\lambda (A_o/bd)^{1/3} > 1.0$ for consuls and cantilever girders
$g_\lambda = 1 + \lambda_v^2$ for $\lambda_v \geq 0.6$ and $g_\lambda = 2.5 - 3\lambda_v > 1.36$ for $\lambda_v < 0.6$
$k_\lambda = 1.0$ for other cases
λ_v is the shear slenderness of a console or a beam section with a free end which the considered section is located = $M_{dmax}/(d \cdot V_{dmax})$
M_{dmax} is the maximum absolute value of M_d in the girder section,
V_{dmax} is the maximum absolute value of V_d in the girder section,
d is the effective height,
A_o is the smallest value of the area of the loading plate or the support. The maximum value should be considered $b \cdot d$. If there are multiple loading plates and supports, A_o is the sum of all areas.
$k_h = 1.6 - h > 1.0$ where h is in meters,
$\omega_o = 100(A_s + A_p)/(b \cdot d) < 2.0$ and $> 0.7 - 0.5 \lambda_v$
b is the web thickness
f_b is design value of long-term characteristic concrete direct tensile strength = mean value of short-term strength/$(1.4)^3$

IV. Rafla 1974

The nominal shear stress τ_{0U} as 5%-fractile of test results is given by the following formula [45].

$$\tau_{0U} = V_U / (0.875 \cdot b \cdot d) = 0.29 \cdot \alpha_u \cdot \alpha_h \cdot (f_{cm})^{1/2} \cdot (\rho)^{1/3} \tag{36}$$

where, V_U is shear resistance and the constants α_u and α_h are given as;

$$\begin{aligned} \alpha_u &= 0.6 - 2.2\,(a/d) && \text{for } a/d \leq 2.0 \\ \alpha_u &= 0.795 + 0.293\,(3.5 - a/d)^{2.5} && \text{for } 2.0 \leq a/d \leq 3.5 \\ \alpha_u &= 0.9 - 0.03\,(a/d) && \text{for } 3.5 \leq a/d \end{aligned} \tag{37}$$

$$\alpha_h = 1/(d/100)^{1/4} \tag{38}$$

2.9. Fracture mechanics

When a notched or cracked specimen of a linear elastic material becomes subjected to load, the region in front of the notch tip (crack) will be highly stressed. A real material cannot stand these high stresses and a damage zone will develop in front of the notch tip. For concrete the damage zone is caused by the development of micro-cracks. The material in this micro-cracked material volume of 'fracture zone' is partly destroyed but is still able to transfer stress. The stress transferring capability normally decreases when the local deformation of the zone increases, i.e. when the number of micro-cracks increases.

The fracture of non-yielding materials is always caused by crack propagation and therefore it was logical when Kaplan [92], started to study the fracture process of concrete by means of fracture mechanics. Since then numerous reports have been published about crack stability, crack propagation and fracture mechanical test methods for concrete and similar materials. Almost all of these publications have one thing in common; concrete is treated as a linear elastic material and the well known *K*- and *G*- approaches, more or less modified are used. A few researches have used other methods such as the *J*-integral approach and *R*-curve analysis.

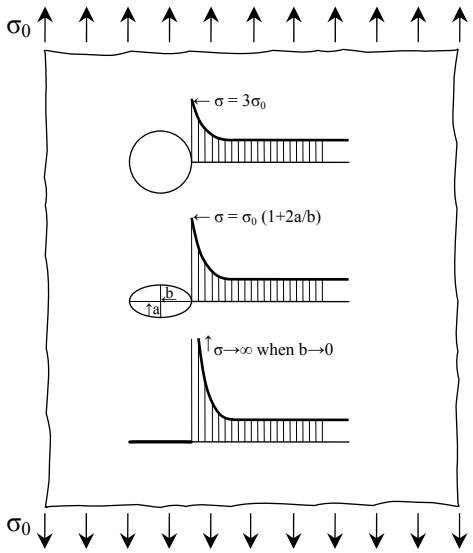

Fig. 26: The stress distributions close to a circular hole, an elliptical hole and a crack in an infinity large plate subjected to the uniform stress σ_0.

Fig. 26 illustrates an infinitely large plate of linear elastic material. The plate is subjected to a uniform tensile stress σ_0. The stress distribution will be disturbed if there is a circular hole in the plate. At the most critical point of the boundary of the hole, the stress will, independently of the size of the hole, reach three times the applied stress. This means that holes or other irregularities will considerably reduce the strength of a material.

If the circular hole is replaced by an elliptical hole, the stress at the tip of the elliptical hole becomes $1+2a/b$ times the applied stress, where a and b are the major and minor axes of the ellipse respectively. If the minor axis is much smaller than the major axis, i.e. $b << a$, then an elliptical hole is a crack and the stress at the crack tip grows unlimitedly as the ratio a/b approaches infinity. This means that ordinary stress criterions cannot be used in this case as the material would then fail as soon as it became subjected to load [93].

A material always contains irregularities. However, a real material is never perfectly linear elastic, at least not at high stresses, and crack tips are never infinitely sharp. These are the reasons why materials can exist at all.

2.9.1. Linear elastic fracture mechanics

Energy criterion

Even if materials never behave perfectly linear elastic it is sometimes possible to approximate the material behaviour with a linear elastic model. As stress criterion cannot be used, one has to use so called fracture mechanics approaches. The first approach of this type was proposed by Griffith [94].

Fig. 27 shows an infinitely large plate subjected to a uniform tensile stress σ_0. The plate contains a $2a$ long crack, which is oriented perpendicular to the applied stress. By equating the elastic strain energy that is released when the crack advances a small distance Δa at each crack tip and the energy necessary to create the new crack surfaces, Griffith found an expression for the critical stress (σ_c) at which the crack propagates:

$$\sigma_c = \alpha\sqrt{\frac{2\gamma E}{\pi a}} \tag{39}$$

where E is he Young's modulus and γ is the surface energy per unit area. α is 1 for plane stress and $[1/(1-\upsilon^2)]^{0.5}$ for plane strain, where υ is Poisson's ratio. For concrete, υ is normally less than 0.2, which means that $1 < \alpha < 1.02$. The discrepancy between plane stress and plane strain is so small for concrete that it can be neglected and below all the relations are relevant for plane stress, i.e. $\alpha = 1$.

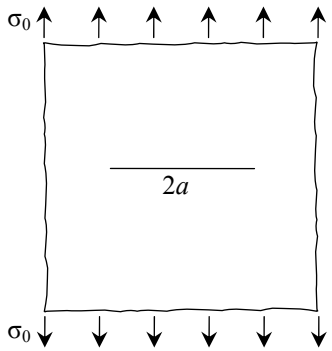

Fig. 27: An infinity large plate with a $2a$ long crack oriented perpendicular to the applied stress σ_0.

By introducing the critical strain energy release rate (G_c), Eq. 39 can be extended to be relevant also for materials where small, irreversible deformations take place close to the crack tip:

$$G_c = \frac{\sigma_c^2 \pi a}{E} \tag{40}$$

G_c includes not only 2γ but also the energy consumption due to deformations close to the crack. The above equation for strain energy is valid for an infinitely large plate. For other specimen geometries and different loading cases it should be multiplied by a correction factor.

Stress intensity criterion

The stress distribution in front of a crack tip, perpendicular to the crack and on a line parallel with the crack, can be expressed as:

$$\sigma = \frac{K}{\sqrt{2\pi x}} + \ldots \tag{41}$$

Where x is the distance from the crack tip and K is the stress intensity factor [93]. The points represent terms that are small compared with the main term for small values of x and therefore the main term itself describes the stress distribution close to the crack tip. As seen in Eq. 41, the stress distribution is unaffected by the geometry of the specimen and the intensity of the stress is only dependent on K. For this reason a stress intensity criterion for initiation of crack growth can be used:

$$K = K_c \tag{42}$$

Where, K_c is the critical stress intensity factor. For the infinitely large plate according to **Fig. 27**, $K = \sigma_0 \sqrt{a\pi}$ and thus:

$$\sigma_c = K_c \Big/ \sqrt{a\pi} \tag{43}$$

By comparing Eq. 43 and 39 it becomes obvious that a connection between K_c and G_c (or K and G) for the infinitely large plate exists:

$$K_c = \sqrt{G_c E} \tag{44}$$

Normally, K_c is expressed as:

$$K_c = \sigma_c \sqrt{a} \cdot f \tag{45}$$

where f is a correction factor dependent on geometry and type of loading. $f = \sqrt{\pi}$ for the infinitely large plate in Fig. 27.

Cohesive zones

In linear elastic fracture mechanics one neglects the fact that the stress at the crack tip theoretically approaches infinity, while the stress in reality can never exceed the cohesive strength of the material. Barenblatt [95] found that a small cohesive zone must exist in a region close to the crack tip, i.e. a zone where closing stresses act between the crack surfaces. Barenblatt assumed the zone to be very small (the length of the zone << length of the crack). Therefore the linear elastic approaches previously discussed can be used for calculation purposes. The existence of cohesive zones explains why linear elastic fracture mechanics can be used at all.

2.9.2. Elastic plastic fracture mechanics

A perfectly linear elastic material follows a straight-lined stress-strain curve all the way to fracture. Even though concrete is a brittle material, the behaviour is not linear elastic. A more realistic stress-strain curve is shown in Fig. 28. The tensile test of concrete shows that the post failure behaviour of the concrete is not totally brittle, but with increasing the strain, there is still some capacity left in a cracked region which could resist small stresses. Hence, the plastic deformation continues with considerably decreasing stress. The material in front of a propagating crack will be highly strained and all the points of the σ-ε curve will be present in the specimen. Three different zones can be separated around the crack tip, see Fig. 29.

1. The linear elastic zone: Far from the crack tip the stress is so low that the material still behaves in a linear elastic way.
2. The plastic zone: In this zone the stress-strain relation is non-linear and the stress increases or at least remains constant as strain increases
3. The fracture zone (process zone): in this zone the stress decreases as the strain increases.

If the plastic zone and the fracture zone are small compared with the specimen dimensions and the crack depth, then linear elastic fracture mechanics can be used. Otherwise, other methods have to be used.

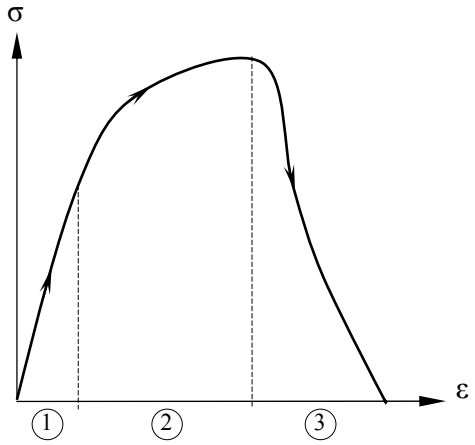

Fig. 28: A schematic illustration of a σ-ε curve. Three parts of the curve can be separated; (1) linear elastic deformations, 2(2) plastic deformations and increasing stress, (3) plastic deformations and decreasing stress.

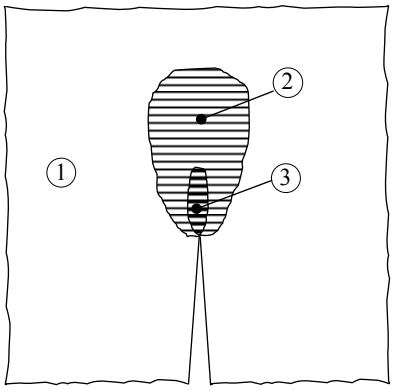

Fig. 29: In front of the crack in a stressed material there is a plastic zone (2) and a fracture zone (3). Far from the crack tip the material behaves in a linear elastic way (1).

2.9.3. The fictitious crack model

By using a very stiff tensile testing machine and a small specimen it is possible to determine the complete tensile stress-strain curve of concrete. An example of such a curve is shown in Fig. 30. At first the material behaves almost linear elastic but when the stress increases, the curve becomes non-linear due to micro-cracks, which are distributed over the entire specimen. When the maximum stress is reached, one cross section is unable to carry more loads. It is fair to assume that the development of micro-cracks will be concentrated in a small material volume close to this cross section when the specimen becomes more deformed. This means that, after the maximum load is reached, additional deformations will take place in the micro-cracked material volume, or fracture zone, while the material outside the fracture zone will be

elastically unloaded. The load decreases when the first fracture zone develops and consequently only a single zone develops.

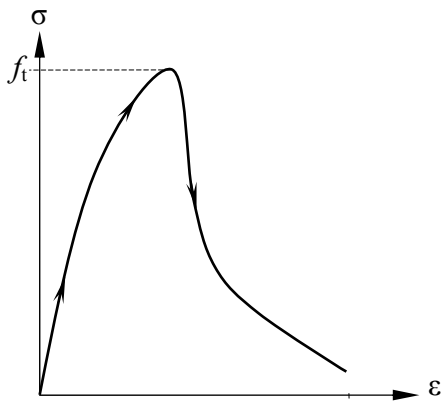

Fig. 30: an example of the complete tensile stress-strain curve for concrete

During the tensile test of a concrete specimen, after the maximum stress is reached, the deformation of the fracture zone affects the mean strain and consequently the stress-strain curve of concrete is dependent on the specimen length. This means that it is unsuitable to use the stress-strain curve as a material property in modelling. A better way of describing the deformation properties of a material therefore is to use two relations; one relation between the stress and the relative strain for the material outside the fracture zone (Fig. 31a) and one relation between the stress and the absolute deformation of the fracture zone (Fig. 31b).

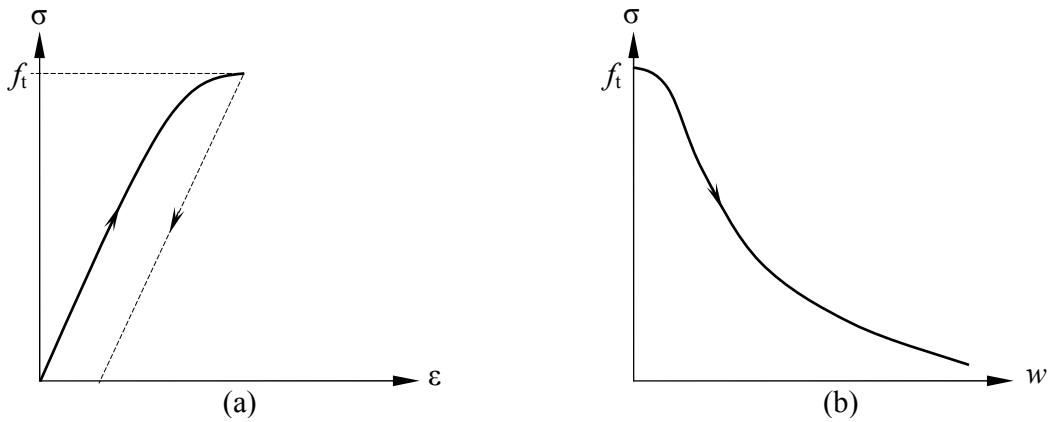

Fig. 31: a) The deformation properties of the material outside the fracture zone are given by a relation between the stress and the relative strain, i.e. a σ-ε curve. b) The deformation properties of the fracture zone are given by a relation between the stress and the absolute widening of the zone in the stressed direction, i.e. a σ-*w* curve

When a notched concrete specimen is subjected to a load, a zone of micro-cracks develops in front of the notch. This fracture zone considerably reduces the stress concentration which [93]results in a much more realistic description of the stress distribution than the linear elastic solution, see Fig. 32.

The fracture zone in front of a notch or a crack normally develops in a tensile stress field and consequently the properties of this zone are similar to those of the fracture zone in a direct tensile test. This means that it should be possible to approximate the fracture zone in front of a notch or crack. The stress transferring capability depends on the width of the slit in the stressed direction. In Fig. 33, the load is represented by a point load but of course this

description is relevant for all types of loads, including volume stresses due to shrinkage or temperature gradients.

The stress transferring crack is not a real crack but can be considered as a fictitious crack and therefore the model described above is called the Fictitious Crack Model. When using the Fictitious Crack Model the following assumptions are made:

- The fracture zone starts developing at one point when the first principal stress reaches the tensile strength of concrete. Of course other more complicated fracture criteria can be used but often the simple tensile strength criteria is sufficient.
- The fracture zone develops perpendicular to the first principal stress.
- The material in the fracture zone is partly destroyed but is still able to transfer stress. The stress transferring capability depends on the local deformation of the fracture zone in the direction of the first principal stress. In the calculations the fracture zone is normally replaced by a stress transferring crack and the stress transferring capability depends on the width of the crack in the stressed direction according to a σ-*w* curve, see Fig. 31b.
- The width of the fracture zone in the stressed direction is assumed to be equal to the widening of the zone, i.e. the width of the zone is zero when it starts developing. For non-yielding materials like concrete this should be a fair assumption.
- The properties of the material outside the fracture zone are given in a σ-ε curve, see Fig. 31a.

The fracture zone starts developing in one point when the first principal stress reaches the tensile strength even if the high stress is due to other reasons than a stress concentration in front of a notch tip or a crack. This means that the Fictitious Crack Model is not a pure fracture mechanics model but initially un-notched structures can also be analyzed. This is one thing that makes the Fictitious Crack Model differ from most approaches. Another advantage is that, by using the Fictitious Crack Model, it is possible to study the development of the fracture zone, the initiation of crack growth and the propagation of the crack though the material. When other models are used, normally only the initiation of crack growth is analyzed [93].

The description of the Fictitious Crack Model above is relevant for a homogeneous material, i.e. a material that has the same properties in all points. In reality no materials are perfectly homogenous, at least not in the atomic scale. However, if the analyzed structure is a few times greater than the largest irregularities in the material, then the material in the structure can be assumed to be approximately homogenous. The σ-*w* curve is then a function of the fraction and the properties of the components of the material.

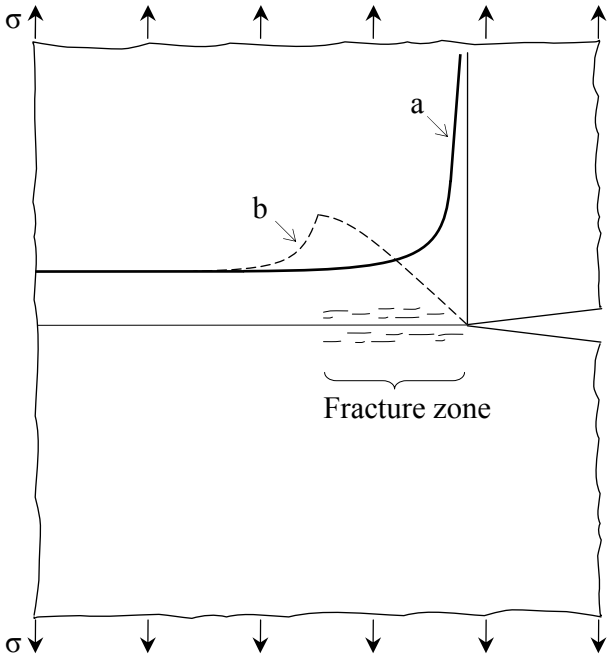

Fig. 32: Probable stress distribution in front of a crack/notch for: a) a linear elastic material b) a non-yielding material with a micro-cracked zone in front of the notch tip [93].

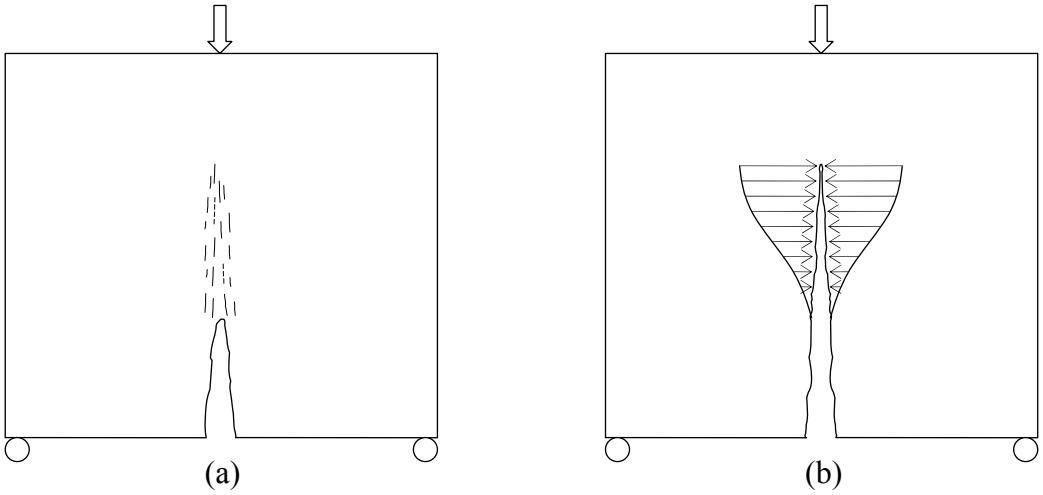

Fig. 33: When using the Fictitious Crack Model, the fracture zone in front of a crack tip (a) is replaced by a crack that is able to transfer stress (b). The stress transferring capability depends on the width of the crack according to a *σ*-*w* curve, see also Fig. 31b.

Chapter 3: Time Dependency

Time dependent effects are caused by for example, superimposed restrained creep, shrinkage, or temperature strains. These additional strains induce a change in the distribution of stresses in the concrete and the steel, resulting in changes in the criteria for a particular structural element at the same external load.

3.1. Development of Strength and modulus of elasticity with time

I. Compressive Strength:
The rate at which concrete strength increases with time depends on a variety of parameters, in particular type strength class of cement, type and amount of admixtures and additions, water/cement ratio and environmental conditions. The development of compressive strength with time may be estimated from Eq. 46 [56].

$$f_{cm}(t) = \beta_{cc}(t) \,.\, f_{cm} \tag{46}$$

where $f_{cm}(t)$ is mean compressive strength [MPa] at a concrete age t [days], f_{cm} is mean compressive strength [MPa] at a concrete age of 28 days and $\beta_{cc}(t)$ is a function to describe the development of the compressive strength with time and can be calculated from Eq. 47.

$$\beta_{cc}(t) = \exp\{s \,.\, [1 - (28t_1/\, t)^{1/2}]\} \tag{47}$$

where t is the concrete age [days], t_1 is 1 day, s is a coefficient which depends on the strength class of cement. With reference to ENV 197-1 (1992) [58], which specifies the CEM cements, the values for the coefficient s may be taken from Table 3.

Table 3: Coefficient *s* for different strength classes of cement, CEB-FIP MC90 [57]

Type of cement	Slowly hardening cements SL	Normal and rapid hardening cements N, R	Rapid hardening high strength cements RS
Strength class of cement	32.5	32.5R 42.5	425.5R 52.5
s	0.38	0.25	0.20

Eqs. (46, 47) are valid for a concrete temperature of 20°C. For a temperature deviating from 20°C a temperature adjusted concrete age should be used.

An Evaluation of Eqs. (46, 47) is shown in Fig. 34 where the ratio $f_{cm}(t)/f_{cm}$ is given as a function of concrete age.

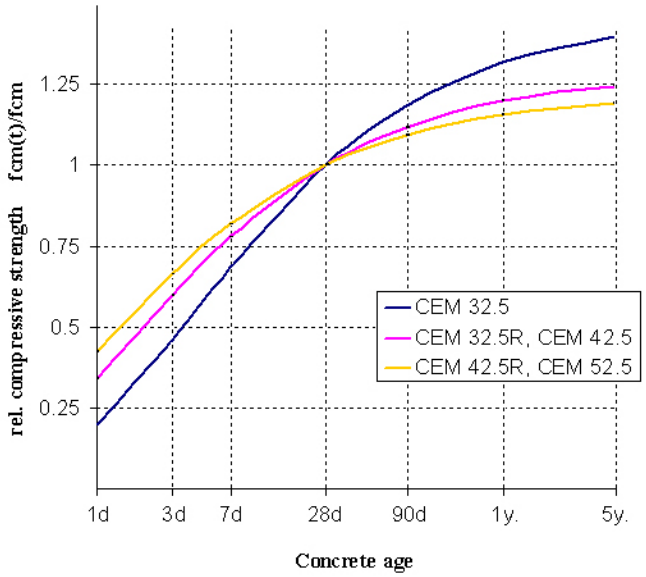

Fig. 34: Development of concrete compressive strength with time at a temperature of 20°C (Eq. 46)

II. Tensile strength

The development of tensile strength with time is much more difficult to predict, because it is influenced significantly by the development of shrinkage stresses which in turn depend on member size and curing conditions. Therefore, only for a concrete age larger than 28 days it may be assumed that the development of the tensile strength with time is similar to that of the compressive strength [59].

III. Modulus of elasticity

The modulus of elasticity of concrete develops more rapidly than does the compressive strength because $E_c(t)$ is to a large extent controlled by the modulus of elasticity of the aggregates which is independent of concrete age. This is taken into account in the following equations [57];

$$E_{ci}(t) = \beta_E(t) \,.\, E_{ci} \tag{48}$$

$$\beta_E(t) = [\beta_{cc}(t)]^{0.5} \tag{49}$$

where, $E_{ci}(t)$ is the tangent modulus of elasticity [MPa] at a concrete age t [days], E_{ci} is the tangent modulus of elasticity [MPa] at a concrete age of 28 days, $\beta_E(t)$ is a function to describe the development of the modulus of elasticity with time, $\beta_{cc}(t)$ is a coefficient acc. to Eq. (47) and t is the concrete age [days]

3.2. Strength and deformation under sustained high loads

I. Compressive Strength

The concrete compressive strength also depends on the duration of loading which it is exposed to a constant stress. This is of practical significance because for many concrete structures the variable load is small compared to the total load, so that the stresses acting on a structural element may vary little with time. A sustained stress in the range of working stress may lead to a slight increase of the compressive strength, found when the concrete is

afterwards loaded to failure in a short-term test [60]. If, however, high sustained stresses act on the concrete, the process of micro-cracking continues and may eventually lead to failure. As the sustained stress decreases, the time to failure increases. The maximum stress, which the concrete can sustain without failure, is referred to as *the sustained load strength*. For a concrete loaded at an age of 28 days it corresponds to approx. 80 percent of its strength under short-term loading.

The sustained load strength depends on the age of concrete at the time of loading, because two effects counteract each other: a high sustained stress causes a strength reduction due to continued micro-cracking, but at the same time the concrete continues to hydrate if a sufficient amount of water is available, resulting in a strength increase. If the rate of strength increase due to continued hydration is more pronounced than the loss of strength due to continued micro-cracking, then failure under the sustained load will no longer occur. This state will be reached sooner, the younger the concrete at the time the sustained stress is applied, because young concrete has a higher potential for continued hydration than older concrete for which hydration may have come to an end at the time of load application.

The period of time during which a concrete may fail under the action of a sustained stress is referred to as the critical period [62]. In CEB-FIP MC90 analytical expressions are given to estimate the strength of concrete under the action of a sustained load depending on the age at loading, the duration of loading and the type of cement;

$$f_{cm,sus}(t,\ t_0) = f_{cm}\,\beta_{cc}(t)\,\beta_{c,sus}(t,\ t_0) \tag{50}$$

$$\beta_{c,sus}(t,t_0) = 0.96 - 0.12\ \{\ln\,[72\ (t - t_0)/t_1\ ]\}^{1/4} \tag{51}$$

where,
f_{cm} is the mean compressive strength of concrete at 28 days,
$f_{cm,sus}(t,\ t_0)$ is the mean compressive strength of concrete at time t when subjected to a high sustained compressive stress at an age at loading $t_0 < t$
$\beta_{cc}(t)$ is a coefficient according to Eq. 47
$\beta_{c,sus}(t,\ t_0)$ is a coefficient which depends on the time under high sustained loads $t - t_0$ (days).
The coefficient describes the decrease of strength with time under load and is defined for $(t - t_0) > 0.015$ days (= 20 min)
t_0 is the age of concrete at loading
$t - t_0$ is the time under high sustained loads (days)
$t_1 = 1$ day

II. Tensile Strength

These shear-carrying mechanisms induce tensile stresses in concrete (Fig. 35) near the crack tip (Zone A) and at the level of the reinforcement (Zone B). In a long-term loading, once the tensile strength of the concrete in Zones A and B is reached, the existing flexural cracks progress in a diagonal direction (Zone A) or new ones are created (Zone B). As a consequence, the capacity of the previous shear-carrying mechanisms (i.e. aggregate interlock and dowel action) is reduced or even cancelled [83].

Tensile strength under sustained loading $f_{ctk,sus}$ in [MPa] can be estimated from:

$$f_{ctk,sus} = \alpha \cdot f_{ctk} \tag{52}$$

where, f_{ctk} is the short-term strength in [MPa] and is α equal to 0.6 for normal strength concrete and 0.75 for high strength concrete.

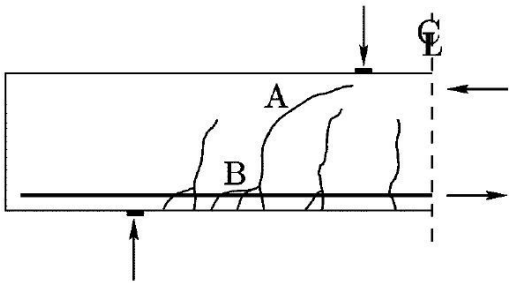

Fig. 35: Shear crack pattern

3.3. Definitions of Time-Dependent Deformations

The time-dependent deformation of concrete, including shrinkage and creep, may cause cracks and has much to do with the durability performance of structural concrete. Creep and shrinkage of concrete are complicated phenomena and it is difficult to formulate a constitutive equation which is both generally applicable and realistic. Before the era of large finite element analysis, this task was not an issue because no structural analysis problems could be solved with a sophisticated constitutive model. Now that finite element analysis can provide the means of solving these problems, there is a need for the development of realistic constitutive relations for long-term loading.

Time-dependent deformations may be stress-dependent or stress-independent. The stress independent strains or volume changes are mainly shrinkage and swelling. The time- and stress-dependent strains are referred to as creep. Such strains are defined as the difference between the increase of strains with time of a specimen subjected to a constant sustained stress and the load independent strain observed on an unloaded companion specimen.

The total strain $\varepsilon_c(t)$ of a uniaxially loaded concrete specimen at age t may be subdivided as;

$$\varepsilon_c(t) = \varepsilon_E(t) + \varepsilon_c(t) + \varepsilon_s(t) + \varepsilon_T(t) = \varepsilon_E(t) + \varepsilon_c(t) + \varepsilon^o(t) = \varepsilon_\sigma(t) + \varepsilon^o(t) \quad (53)$$

where,
$\varepsilon_E(t)$ is the instantaneous strain, which is elastic (reversible) if the stress is small,
$\varepsilon_c(t)$ is the creep strain at concrete age t,
$\varepsilon_s(t)$ is the shrinkage (or swelling) at concrete age t,
$\varepsilon_T(t)$ is the thermal expansion (or dilatation),
$\varepsilon^o(t)$ is the stress-independent inelastic strain,
$\varepsilon_\sigma(t)$ is the stress-produced strain, also called the mechanical strain.

The strain $\varepsilon_E(t)$ is irreversible due to aging caused by hydration, as well as by other time-dependent changes in the microstructure. It should be kept in mind that the distinction between creep as a stress-dependent strain and shrinkage or swelling as stress independent strains is conventional and in times useful to facilitate analysis and design.

Shrinkage

Concrete undergoes volume changes during hardening. As concrete continues to dry, water evaporates and the volume of the restrained cement paste changes, causing concrete to shrink, probably due to the capillary tension that develops in the water remaining in concrete. Emptying of the capillaries causes a loss of water without shrinkage, but once the absorbed water is removed, shrinkage occurs. This deformation occurs when ordinary hardened concrete is exposed to air with a relative humidity of less than 100 percent. However, there exist several other types of shrinkage deformations, such as plastic shrinkage, autogenous shrinkage and carbonation shrinkage which may occur simultaneously and which are added up as total shrinkage.

Plastic shrinkage occurs when water is lost from concrete while it is still in plastic state. *Autogenous shrinkage*, also called *self-desiccation shrinkage* or *chemical shrinkage*, is associated with the ongoing hydration reaction of cement. *Carbonation shrinkage* is caused by the reaction of hydrated cement paste with carbon dioxide in the air in the presence of moisture. Among the different types of shrinkage, drying shrinkage is the most important type of shrinkage in concrete practice.

Total shrinkage after long duration of drying ranges from about 0.0001 to 0.001. For normal strength concrete the most important parameter influencing the magnitude of shrinkage is the water loss after a given duration of drying.

The model presented below predicts the mean time-dependent shrinkage behaviour of a plain structural concrete member which is exposed to a dry or to a moist environment after curing. It is valid for normal and for high-performance concrete up to a strength of 120 MPa, moist cured at normal temperatures not exceeding 14 days and exposed to a mean relative humidity in the range of 40 to 100 percent.

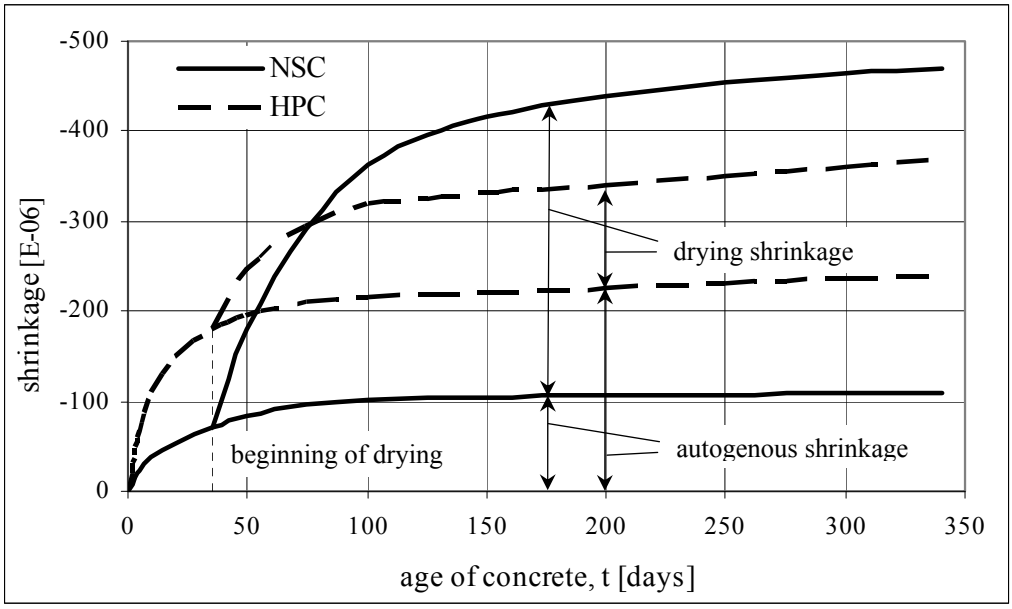

Fig. 36: Time development of autogenous shrinkage and of drying shrinkage in normal strength concrete and in high-performance concrete

It should be pointed out that the prediction models for shrinkage as well as for creep given in CEB-FIP MC90 and Bažant [65] include compressive strength as a major parameter to be

taken into account when estimating concrete deformation properties. In reality, shrinkage and creep strains per se do not depend on concrete compressive strength but rather on parameters related to the microstructure and concrete composition such as water/cement ratio, degree of hydration, properties of the aggregates, etc.

The total shrinkage may be calculated from;

$$\varepsilon_s(t, t_s) = \varepsilon_{as}(t) + \varepsilon_{ds}(t, t_s) \tag{54}$$

$$\varepsilon_{as}(t) = \varepsilon_{aso}(f_{cm}) \,.\, \beta_{as}(t) \tag{55}$$

$$\varepsilon_{ds}(t, t_s) = \varepsilon_{dso}(f_{cm}) \,.\, \beta_{RH}(RH) \,.\, \beta_{ds}(t - t_s) \tag{56}$$

$$\varepsilon_{aso}(f_{cm}) = - \alpha_{as} \left[(f_{cm}/f_{cm0}) / (6 + f_{cm}/f_{cm0})\right]^{2.5} \,.\, 10^{-6} \tag{57}$$

$$\beta_{as}(t) = 1 - \exp[- 0.2 \, (t/t_1)^{0.5} \,] \tag{58}$$

$$\varepsilon_{dso}(f_{cm}) = [(220 + 110 \, \alpha_{ds1} \,) \,.\, \exp(-\alpha_{ds2} \,.\, f_{cm} / f_{cmo} \,) \,] \,.\, 10^{-6} \tag{59}$$

$$\beta_{RH}(RH) = - 1.55 \, [\, 1 - (RH / RH_o)^3 \,] \quad \text{for RH} < 99\% \,.\, \beta_{s1} \tag{60}$$
$$\beta_{RH}(RH) = 0.25 \quad \text{for RH} < 99\% \,.\, \beta_{s1}$$

$$\beta_{ds}(t - t_s) = [(t - t_s)/t_1]^{0.5} / [350 \, (h / h_o)^2 + (t - t_s)/t_1 \,]^{0.5} \tag{61}$$

$$\beta_{s1} = (3.5 \, f_{cm0} / f_{cm})^{0.1} \tag{62}$$

where,

$\varepsilon_s(t, t_s)$	total shrinkage at time t
$\varepsilon_{as}(t)$	autogenous shrinkage at time t
$\varepsilon_{ds}(t, t_s)$	drying shrinkage at time t
$\varepsilon_{aso}(f_{cm})$	national autogenous shrinkage coefficient
$\varepsilon_{dso}(f_{cm})$	national drying shrinkage coefficient
$\beta_{as}(t)$	function to describe the time development of autogenous shrinkage
$\beta_{RH}(RH)$	coefficient to take into account the effect if rel. humidity on drying shrinkage
$\beta_{ds}(t - t_s)$	function to describe the time development of drying shrinkage
β_{s1}	coefficient to take into account self-desiccation in high-performance concretes
f_{cm}	mean compressive strength [MPa]
f_{cm0}	= 10 MPa
α_{as}	coefficient which depends of the type of cement: α_{as} = 800 for slowly hardening cements α_{as} = 700 for normal or rapid hardening cements α_{as} = 600 for rapid hardening high-strength cements
α_{ds1}	coefficient which depends of the type of cement: α_{ds1} = 3 for slowly hardening cements α_{ds1} = 4 for normal or rapid hardening cements α_{ds1} = 6 for rapid hardening high-strength cements
α_{ds2}	coefficient which depends of the type of cement: α_{ds2} = 0.13 for slowly hardening cements α_{ds2} = 0.11 for normal or rapid hardening cements α_{ds2} = 0.12 for rapid hardening high-strength cements

RH	ambient relative humidity [%]
RH_o	= 100 %
t	concrete age [days]
t_1	= 1 day
t_s	concrete age at the onset of drying [days]
$t - t_s$	duration of drying [days]
h	= 2 A_c/u national size of member [mm], where A_c is the cross-section [mm^2] and u is the perimeter of the member in contact with atmosphere [mm]
h_o	= 100 mm

Creep

Creep is quantified in terms of the strain that occurs in addition to the elastic strain due to the applied loads. If the applied loads are close to the service loads, the creep strain increases at a decreasing rate with time. The ultimate creep strain is found to be proportional to the elastic strain. The ratio of the ultimate creep strain to the elastic strain is called the creep coefficient.

Creep of concrete is very much dependent on stress level. Beginning with small stresses, plastic strains in concrete develop in addition to elastic ones. Under sustained load, plastic deformation continues to develop over a period that may last for years. Such deformation increases at high rate during the first four months after application of the load. This slow plastic deformation under constant stress is called creep.

In the range of service stresses, i.e. $\sigma_c \leq 0.4 f_{cm}$, concrete may be considered as an ageing linear viscoelastic material. Hence, creep strains are linearly related to stress and can be calculated from;

$$\varepsilon_c(t, t_0) = \varphi(t, t_0) \,.\, \sigma_c\,(t_0) / E_{ci} \tag{63}$$

where,

$\varepsilon_c(t, t_0)$	creep strain at time t of a concrete loaded at an age t_0
$\varphi(t, t_0)$	creep coefficient
$\sigma_c\,(t_0)$	creep inducing stress, i.e. stress applied at time t_0
E_{ci}	modulus of elasticity at concrete age of 28 days which can be calculated from;

$$E_{ci} = \alpha_E \,.\, E_{co}\,(f_{cm} / f_{cmo})^{1/3} \tag{64}$$

where,

E_{ci}	tangent modulus of elasticity at σ_c = 0 [MPa] and at a concrete age of 28 days
E_{co}	= 2.15×10^4 MPa
f_{cm}	mean compressive strength [MPa]
f_{cmo}	= 10 MPa
α_E	coefficient from Table 4

Table 4. Effect of type of aggregate on modulus of elasticity of concrete [57]

Type of aggregate	α_E
Basalt, Dense limestone	1.2
Quartzitic aggregates	1.0
Limestone	0.9
Sandstone	0.7

Creep of concrete may affect the long-term behaviour of concrete structures both in favourable and unfavourable way. When subjected to sustained load, the deformations of a concrete structure will continue to increase due to the effects of creep. According to Rüsch et al. [68], the deflection of a reinforced concrete member subjected to flexure, $d(t)$, increases with time;

$$d(t) \approx d_i \, [\, 1 + 0.3 \, \varphi(t, t_0) \,] \tag{65}$$

where d_i is the initial deflection. In reinforced concrete sections subjected to compression, creep of concrete causes a redistribution of stresses from the concrete to the reinforcing steel which may lead even to yielding of the steel [59].

The creep coefficient $\varphi(t, t_0)$ of a concrete at age t which has been subjected to a constant sustained load at an age t_0 follows from;

Uniaxial elastic creep (stresses less than about 0.4 of the strength) is defined as;

$$\varepsilon(t) = \sigma \, J(t,t') + \varepsilon^{o}(t) \tag{66}$$

in which σ represents the uniaxial stress, ε is axial strain, t is time, normally chosen to represent the age of concrete, and $J(t,t')$ is the compliance function (often also called the creep function); this function represents the strain (elastic plus creep) and the time t caused by a unit constant uniaxial stress that has been acting since time t'. Within the linear range, the creep at uniaxial stress is completely characterized by function $J(t,t')$.

The creep of concrete is profoundly influenced by the process of cement hydration. This influence is called aging and causes the creep at constant stress to decrease significantly as the age at loading increases. Modeling of the aging aspect of creep has proven to be a major complicating factor. Although integral as well as differential formulations that take the aging into account are available and used in practice, they have several serious shortcomings. The objective of this theory is to eliminate these shortcomings with a basic model proposed by Bażant and Parasannan [55]. The theory has a physical basis in the micromechanics of the aging process. The formulation has several important advantages: It involves a Kelvin chain whose elastic modulus and viscosities are age-independent, which greatly simplifies numerical analysis. All the free material parameters can be identified from the given test data by linear regression. All the viscoelastic behaviour of concrete, including aging, can be closely described with only four free material parameters. The model always satisfies the condition of non-divergence of the creep curves for different ages at loading. Thermodynamic restrictions for the elastic module and viscosities associated with the rate-type form are always satisfied. The non-linearity of creep consisting in deviations from the principle of superposition is capable of describing the phenomenon of adaptation and agrees with test data for the service stress range as well as higher stresses.

The creep-time curve may include three ranges: primary creep, secondary creep and tertiary creep (Fig. 37). In the secondary creep range, the creep rate is approximately constant. This it is also called stationary creep or steady state creep. The tertiary creep may arise under high applied stresses.

The creep-time curve is dependent on the stress-strength ratio. Below a stress-strength ratio of about 0.4 it is proportional to the applied stress. It appears that the initial rate of creep in

tension is higher than that in compression under the same stress; at longer time the reverse may be true according to Illston [102]. The effect of the stress-strength ratio seems similar to the effect in case of compressive creep: creep is proportional to the applied stress up to 0.5, even higher.

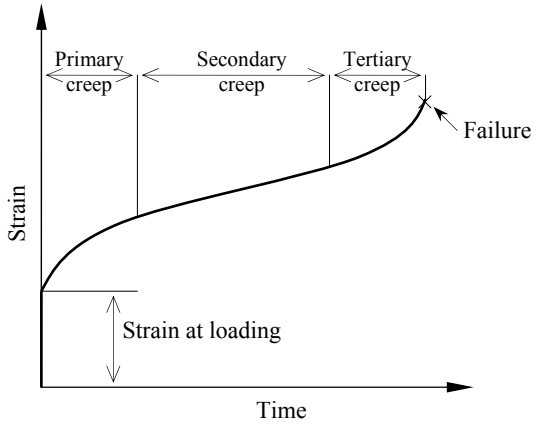

Fig. 37: Schematic creep-time curve [100]

Stress Relaxation

Although the term creep is often used to denote both the phenomenon of creep deformation and that of relaxation of stress, they are of course not the same, but different manifestations of the same fundamental viscoelastic properties. If a structural concrete member can freely deform under a permanent constant stress, its deformation increases due to creep. If free development of creep deformation is prevented, then the original stress is reduced over time, i.e. relaxation takes place [97].

The relaxation in concrete specimens subjected to equal initial strains at different ages of concrete is illustrated in Fig. 38. It shows that the stress decreases at a higher rate in younger concrete analogous to the creep behaviour. The difference in relaxation of the initial stresses has a relation to the increase of the modulus of elasticity with time. Comparing the stress relaxation magnitudes $\Delta\sigma_1$, $\Delta\sigma_2$ and $\Delta\sigma_3$ after a time increment Δt from the loading time t_i it is clear that the relaxation is very high at early ages and it reduces with time, just as creep reduces with age at loading.

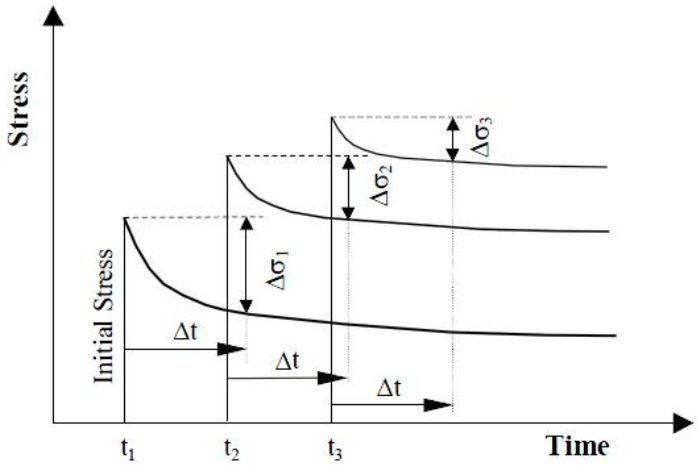

Fig. 38: Effect of loading age on relaxation in concrete specimens subjected to equal initial strains [97].

The development of the relaxation process at different levels of the initial stress is plotted in Fig. 39. Compared to creep, the process of relaxation develops more rapidly at the beginning and approaches its final value asymptotically. It shows also that the relative increase of relaxation is higher than the relative increase of stresses above 11.8 MPa, i.e nonlinearity of relaxation appears. Due to the lack of data on stress relaxation at early ages, the findings concerning the development of creep are used in most of the theoretical studies of stress analysis for the modelling. The linear viscoelastic theories allow calculation of relaxation based on creep data.

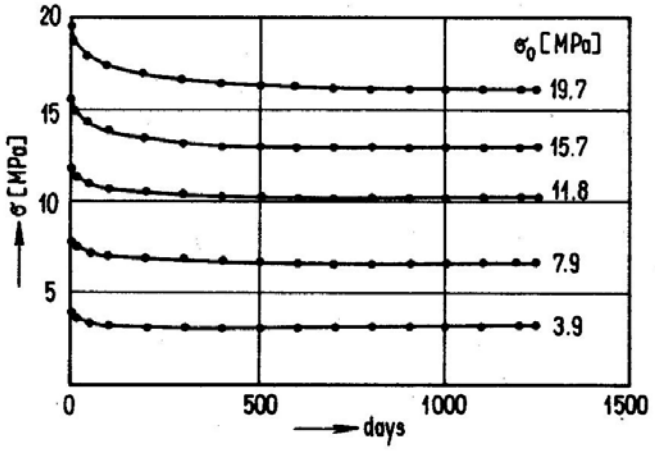

Fig. 39: Effect of magnitude of the initial stress on the relaxation process [98].

Chapter 4: Modelling

The theoretical researches before 1990 focused on the development and formulation of suitable and realistic constitutive laws, describing the observed mechanical behaviour of concrete [2,3,24,25,26]. The primary purpose of these efforts was the implementation of the numerical models in finite element programs aimed at simulating and computing the behaviour of complicated reinforced concrete structures. The finite element method offers a model of the structure consisting of an assemblage of simple elements for the in-plane shear transfer in cracked concrete. The displacement response of the crack is complex and highly non-linear: analytical expressions approximating the test data can often be formulated by means of statistical methods.

Two extreme crack response curves can be distinguished for the case of a displacement-controlled shear loading [23], namely retaining a constant crack width, related to an infinite normal stiffness of the crack plane, or a constant normal stress which can be achieved by a constant external normal force together with a zero normal stiffness, see Fig. 40.
In actual structures the crack plane is often partially constrained by means of reinforcing bars crossing the crack. Apart from a certain normal stiffness $d\sigma_c/d\delta_n$, the dowel and aggregate interlock mechanisms provide a shear stiffness $d\tau/d\delta_t$. In Fig. 40 δ_t is slip or parallel displacement of two sides of the crack and δ_n is separation or crack width.

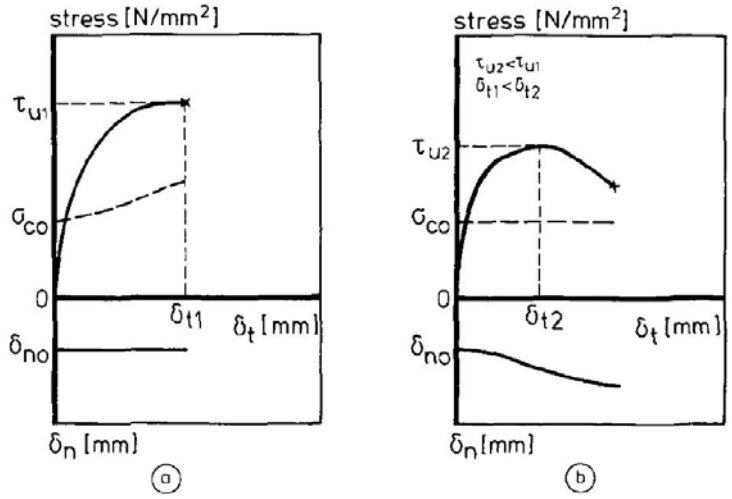

Fig. 40: Shear stress-displacement behaviour of a crack for (a) constant crack width and (b) constant normal stress

One empirical shear stress-displacement relation was found for the variable crack width tests (constant stress-crack width ratio) by Paulay and Loeber [63]:

$$\tau_a = 0.51 + 7.07(\delta_t)^{1/2} \tag{67}$$

where, τ_a is shear stress and δ_t is slip or parallel displacement of two sides of the crack.

Paulay and Loeber carried out displacement-controlled (with respect to δ_t) static shear loading tests, see Fig. 27a. The crack width, slip and restraining stress perpendicular to the crack plane were recorded. Three types of gravel aggregate (rounded: 9.5 mm and 19 mm max. size and

crushed: 19 mm), as well as three different constant crack widths were chosen as experimental variables. The 102 mm cube concrete strength ranged between 36 and 40 N/mm^2.

This formula resembles well with the predicted curve as derived from the constant crack width tests, see Fig. 27b. Houde and Mirza [50] performed similar push-off tests and found that τ_a is almost proportional to $f_{cyl}^{1/2}$ and $\delta_{no}^{1.5}$.

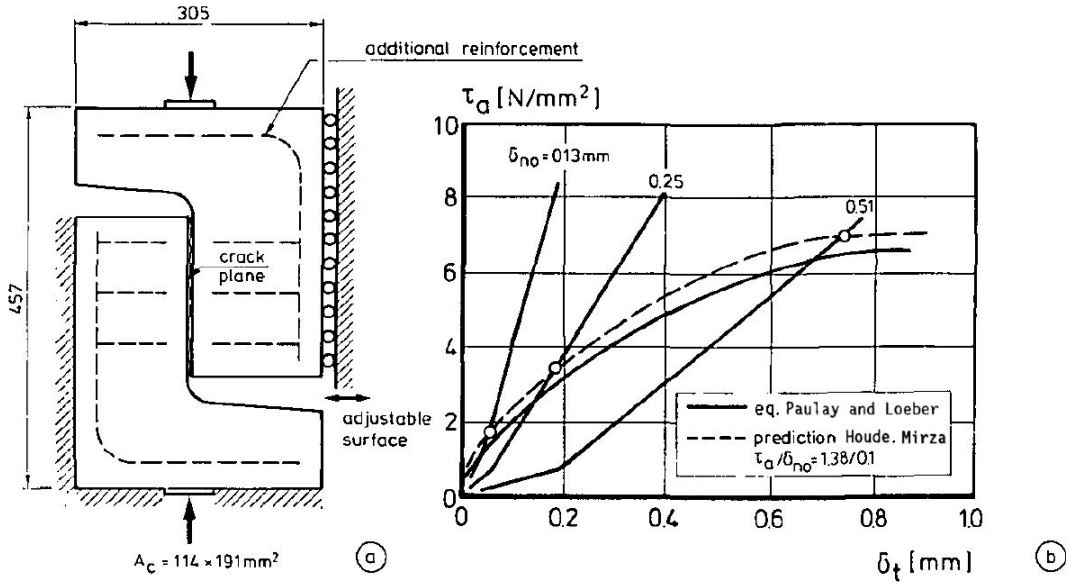

Fig. 41: Test set-up by Paulay and Loeber and (b) relations for concrete (D = 19mm).

A theoretical model should consider the interaction between the stresses and displacements (σ, τ, δ_n, δ_t). In this section, a few theoretical models will be reviewed:

4.1. Rough-crack model of Bažant and Gambarova

This model gives a mathematical description of the observed crack behaviour [64-66]. The interface stresses are assumed to depend on the displacement ratio R = δ_t/δ_n. Free sliding can occur (σ_a = 0) until both crack faces make contact. The maximum shear stress is stipulated by the crushing of mortar material (Fig. 42). The aggregate particles have a Fuller grading curve. The formulae presented are based on shear tests of Paulay et al. [63]:

$$\tau_a = 0.25 f_{cyl} \cdot (1 - \sqrt{2\delta_n / D_{\max}}).R.\frac{a_3 + a_4 \cdot |R|^3}{1 + a_4 \cdot R^4} \tag{68}$$

$$\sigma_a = -a_1 \cdot a_2 \cdot \tau_a \sqrt{\delta_n}.\frac{R}{(1+R^2)^{0.25}} \tag{69}$$

where a_1, a_2, a_3 and a_4 are constant values related to f_{cyl}. Note that τ_a has a boundary value of $0.25 f_{cyl}$. The crack-opening curves are restricted to $\delta_t = c \cdot \delta_n^a$ ($a > 1$). The model does not describe shear transfer in reinforced cracks due to lack of reliable test data. Later, the model was used to determine the contribution of aggregate interlock to the shear transfer of cracked reinforced concrete beams [73].

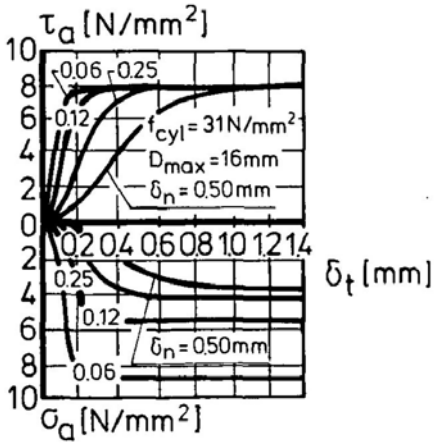

Fig. 42: Calculated response according to Eq. 69

4.2. Two-phase model of Walraven

Walraven et al. [74], [75] used 32 push-off type specimens as shown in Fig. 43a. By means of nuts the external restraint rods were fastened to stiff steel plates fixed on the small sides of the specimens. Dowel action of these bars was negligible. The shear loading was applied in a displacement-controlled manner. The variables of the tests were: initial crack width (0.01, 0.2 and 0.4 mm), 150 mm cube strength and type of aggregate (Fuller grading curve, gravel: f_{cc}=19.9-56.1 N/mm^2, Korlin light-weight aggregates: f_{cc} = 38.2 N/mm^2) and the maximum size (16mm but D_{max}=32 mm for the high-strength type of concrete). The change of the rod diameter enabled variation of the normal stiffness to the crack plane. The test results of six specimens are presented in Fig. 43b; δ_n had a considerable influence, but there was a rather slight effect on τ_a-δ_t relations of D_{max} in the range tested. Empirical bilinear stress-displacement relations were found which accurately fit to the data recorded:

$$\tau_a = -\frac{f_{cc}}{30} + [1.80\delta_n^{-0.80} + (0.234\delta_n^{-0.707} - 0.20)\cdot f_{cc}]\cdot\delta_t \qquad [\text{N/mm}^2] \quad (70)$$

$$\sigma_a = -\frac{f_{cc}}{20} + [1.35\delta_n^{-0.63} + (0.191\delta_n^{-0.552} - 0.15)\cdot f_{cc}]\cdot\delta_t \qquad [\text{N/mm}^2] \quad (71)$$

Similar equations were obtained for the light-weight concrete which exhibited a less steep crack-opening curve indicating a relatively smooth crack surface, probably caused by cracks that run mainly through the aggregate particles which are weaker than the matrix material.

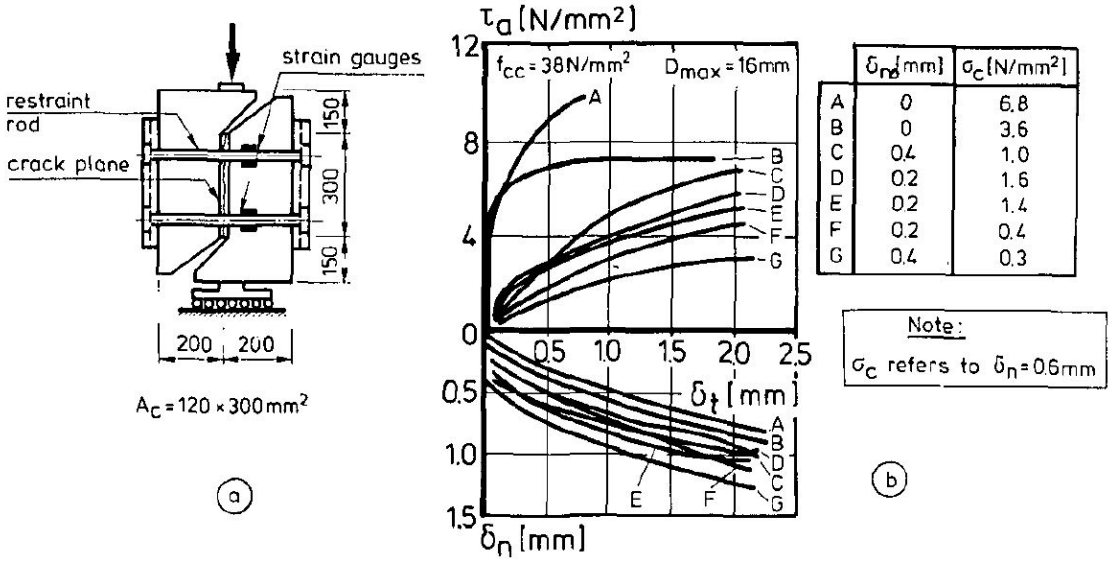

Fig. 43: Tests of Walraven et al. [74],[75]; (a) specimen with external restraint rods and (b) shear stress-displacement relations and measured crack-opening curves for normal-weight concrete.

Based on these tests, Walraven presents a model which suggests that concrete is a two-phase material consisting of stiff aggregate particles embedded in an ideally-plastic cement matrix (Fig. 44a-b). In gravel concrete the low bond strength between the matrix and these particles may usually lead to crack initiation. The particles are idealized as spheres. The shear plane consists of a distribution of rigid spheres of a range of sizes embedded to various depths in the matrix material. The model does not consider interaction between spheres from opposite crack faces. An expression is derived to predict the chances of finding a particular sized aggregate particle at a certain embedment depth. Equilibrium is related to frictional sliding and crushing of matrix along the contact areas a_x and a_y (Fig. 44c), which depend on δ_t, δ_n and the mix proportions (D_{max} and the volumetric percentage of aggregate). A Fuller grading curve is used for the particle distribution. The constitutive relations of the crack are unique - i.e. there is path-independency - ace. to:

$$\sigma_a = \sigma_{pu} \cdot (A_x - \mu \cdot A_y) \quad \text{and} \quad \tau_a = \sigma_{pu} \cdot (A_y + \mu \cdot A_x) \qquad [N/mm^2] \quad (72)$$

where,
$\mu = \tau_{pu}/\sigma_{pu}$ = coefficient of friction = 0.40
σ_{pu} = matrix yield strength = $6.39 f_{cc}^{0.56}$ [N/mm²]
$A_x = \Sigma a_x$, $A_y = \Sigma a_y$ = contact areas per unit area of crack plane.

The model closely agrees with Walraven's static shear tests (Fig. 43b) and with the experiments of Paulay et al. [63] for a given normal restraint 'stiffness' of the crack plane. From Eq. 72, Fig. 44d can be drawn. It can be seen that the 'free slip' at $\sigma_a = 0$ increases as the initial crack-opening is enlarged. Simple bilinear expressions have been derived according to Eqs. (70-71). A further analysis revealed that the path-dependency of the interlock mechanism can almost be neglected if $\delta_t < \frac{2}{3} \delta_n$ [76]. Note that Walraven combined the aggregate interlock and the dowel mechanisms in order to simulate the response of cracked reinforced push-off specimens.

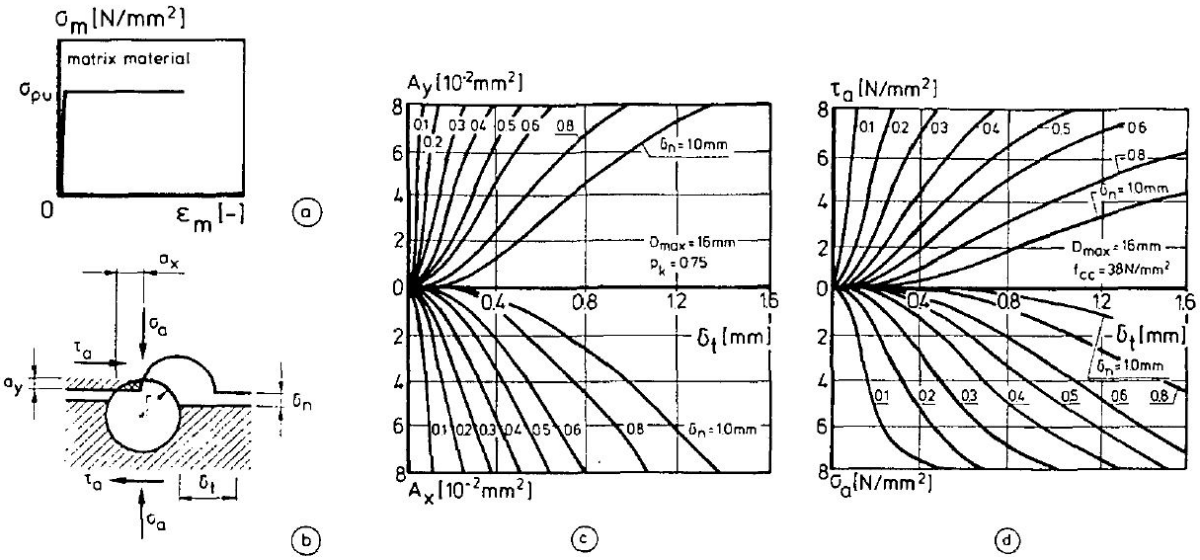

Fig. 44: Model of Walraven [75]; (a)-(b) assumed matrix deformation;(c) contact areas and (d) stresses for a single crack.

4.3. Model of Wittmann and Zaitsev

Wittmann and Zaitsev [80] modelled theoretically the opening of the crack under short-term and long-term compressive loads, see Fig. 45.

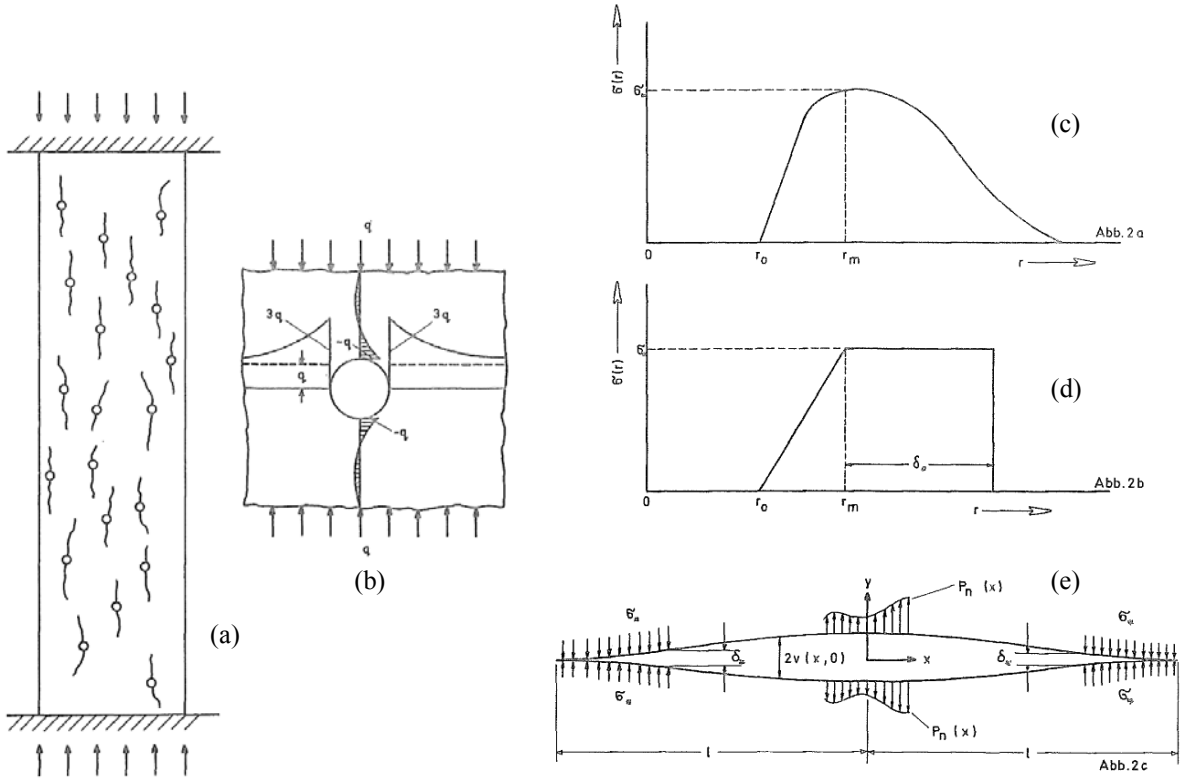

Fig. 45: a) Crack propagation in porous material under compression. b) Stress distribution in a homogeneous material around a circular hole under uniaxial compression. c) Schematic representation of the stress σ between two particles of a solid body as a function of your distance. d) Theoretical model for stress between two particles. e) Schematic representation of a crack in a solid body, when the crack width is more than δ_* the tensile forces between two faces of the crack is gone [80]

Based on their model, the simplest element to in an idealized structure of a porous material is a circular hole in a homogeneous and isotropic plate. In Fig. 45 the well known stress distribution around a circular hole is shown. As soon as the tensile strength of the material at the lines of maximum tensile stress is reached a crack will propagate into the material. It can be shown that the related crack length λ is dependent on the applied load q by the following expression:

$$q = \sqrt{\frac{\pi E \gamma}{2r}} \sqrt{\frac{(1+\lambda)^7}{(1+\lambda)^2 - 1}} \tag{73}$$

where λ is equal to the crack length l divided by the radius of the pore r. All other symbols in equation (1) have their usual meaning.

Equation (73) can be applied when the crack length l is small compared to the distance of individual pores. That means, when the interaction between two mutual approaching cracks is negligible. This is, of course, a severe limitation of the mathematical description. Zaitsev and Wittman, therefore, studied the crack propagation of two interfering cracks and finally the crack propagation in a material with pores distributed at random. In this model which is fairly close to a realistic porous structure, the sum of the length of all individual micro-cracks has been calculated. Each time two pores become connected by the merging of two increasing cracks there is a sudden increase in the total crack until a critical value is reached. Then the cracks propagate without any increase in load.

If the material is viscoelastic cracks can propagate due to the fact that creep occurs in the immediate vicinity of the crack tips. Čerepanov [104] has shown that formulas which are derived under the assumption that a material reacts in an ideal way can be extended so that they can be applied to describe the behaviour of a viscoelastic material as well. In this case the elastic modulus E has to be replaced by a time dependent operator $\check{E}$ where:

$$\frac{1}{\tilde{\mathrm{E}}} = \frac{1}{E} + \int_{\tau 1}^{t} K(t,\tau) \frac{\sigma(\tau)}{\sigma(t)} \frac{1}{E(\tau)} d\tau \tag{74}$$

where $K(t, \tau)$ has the following meaning:

$$K(t,\tau) = -E(\tau) \frac{\partial}{\partial(\tau)} \left[\frac{1}{E(\tau)} + c(t,\tau) \right] \tag{75}$$

Now it is possible to calculate the time t when a specimen fails under a high sustained load, the load being applied at time τ. The basic assumption here is that the specimen will fail as soon as the total crack length increases due to creep of the material in the crack tips and reaches a value that equals the critical crack length of the short time experiment. The related strength under sustained load is then given by the following expression:

$$\eta(t,\tau) = \frac{m(t,\tau)\beta_K(t)}{\beta_K(\tau)} \sqrt{\frac{E(\tau)}{E(t)} \cdot \frac{1}{1+\varphi(t,\tau)}} \tag{76}$$

$\beta_K(t)$ and $\beta_K(t)$ being the short time strength of a companion specimen at time t when the sample fails and at time τ when the load has been applied respectively. $E(t)$ and $E(\tau)$ represent the elastic modulus at the indicated age.

Creep in the material near the crack tips not only increases the crack length but reduces the stress concentration at the same time which leads to an increase in strength, $m(t, \tau)$ takes this effect into consideration. Further theoretical and experimental investigations are needed to understand the m-effect in full detail.

4.4. Dugdale model

Dugdale [96] presented a crack model for an elastic-ideal plastic material. Even though the concrete is a brittle material, many approaches to crack analysis based on a single crack concept are based on Dugdale model or Barenblatt model [95].

For an elastic-ideal plastic material the stress can never exceed the yield stress. In the model according to Dugdale it is assumed that a narrow yield zone develops in front of the crack tip along the line of the crack, see Fig. 46. The stresses in the yield zone never exceed the yield stress and consequently load-case (a) in Fig. 46 equals the sum of the load-cases (b) and (c).

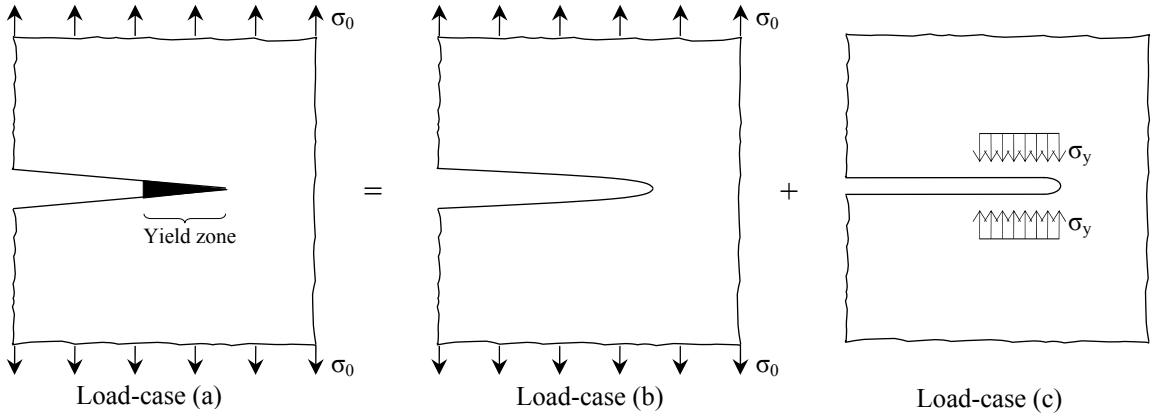

Fig. 46: Dugdale model of a single crack for elastic-ideal plastic material

4.5. FE Model of Petersson, Hillerberg and Modéer

Petersson, Hillerberg and Modéer [93] developed the Fictitious Crack Model based on Dugdale [96] and Barnblatt [95] models. The basic idea of their model is demonstrated in Fig. 47a. When using Finite Element Method (FEM), they modelled the fracture zone by 'nodal forces'. The closing stresses acting across the fracture zone (Fig. 47a) are replaced by nodal forces (Fig. 47b). The intensity of these forces of course depends on the width of the Fictitious Crack according to the σ-w curve of the material. When the tensile strength or another fracture criterion is reached in the top node (Fig. 47b), this node is "opened" and forces start acting on the crack at this point. In this way it is possible to follow the crack growth through the material.

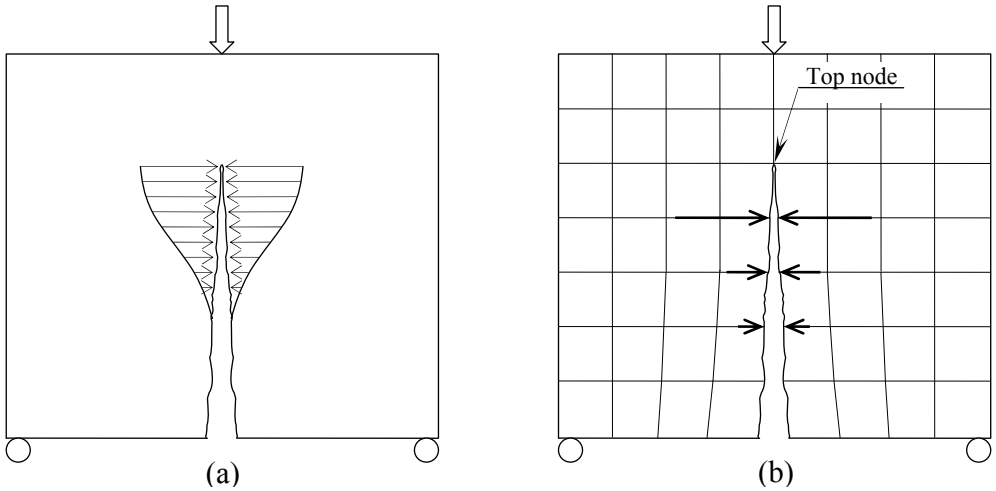

Fig. 47: When using FEM, the stresses acting the Fictitious Crack (a) are replaced by nodal forces (b)

In Fig. 48 a schematic illustration of a deeply cracked structure that is subjected to load is shown. This type of structure is used as the basis in Petersson's calculation method [93]. The dots on the boundaries of the crack represent finite element nodes. The position of the two nodes in each node pair (a node pair is two nodes on the opposite crack surfaces at the same distance from the crack tip) will coincide when the structure is unloaded. The node pairs are numbered from 1 at the base of the crack to n+1 at the crack tip. The distance between two pairs of nodes i and i+1 is denoted a_i.

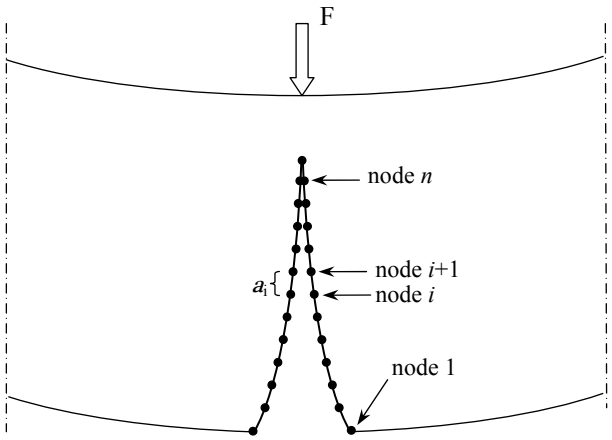

Fig. 48: A schematic illustration of the finite element nodes along the crack boundaries in a deeply cracked specimen [93]

By introducing closing forces over the crack it is possible to make the structure in Fig. 48 relevant for an arbitrary notch depth. If the material is linear elastic and if the deformations are small, the widening of the crack at each node point from node 1 to node n can be expressed by n equations:

$$w_i = \sum_{j=1}^{n} K(i,j)P(j) + C(i)F + w_V(i) \tag{77}$$

where,

$w(i)$ is the width of the crack at node i

$w_I(i)$ represents the separation of the nodes in the node pair i,
F is the load applied to the structure,
$P(j)$ is the closing force acting at node j,
$K(i,j)$ is widening of the crack at node i of the structure in Fig. 48 when unity load is acting at node j
$C(i)$ is the widening of the crack at node i of the structure when the applied load equals unity load.

If the crack propagation path is known in advance, then the values of constants $K(i,j)$, $C(i)$, $D(i)$ and D_F are known as well by means of finite element calculations. When determining the constants a number of different load cases are solved but the same global stiffness matrix can be used for all the load cases and consequently it is only necessary to carry out a single invertation of the stiffness matrix.

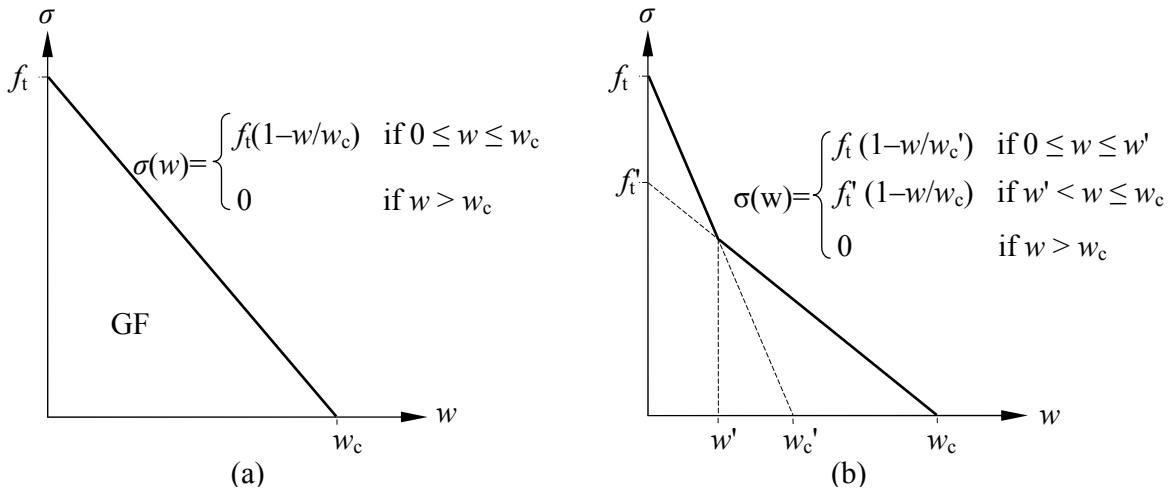

Fig. 49: a) The simplest approximation of the *σ-w* is a single, descending, straight line. b) The *σ-w* curve approximated with two straight lines [93].

Sometimes it is impossible to predict the crack propagation path in advance, so a super position principle should be used. Here the first step is to apply the load F_1 to the linear elastic structure which gives the stress $\sigma(1, i)$ in each node i. The load F_1 is chosen so that the tensile strength is reached at the crack tip i.e. $\sigma(1, 1) = f_t$. The second step is to "open" node 1 and to introduce opening forces across the crack at this mode. The intensity of the forces must depend on the width of the Fictitious Crack according to the σ-w curve and the area which is represented by the forces. For the simple straight-lined σ-w curve in Fig. 49a, the intensity of the forces increases linearly from 0 to $a_1 \cdot b \cdot f_t/2$ when w increases from 0 to w_c. The forces are 0 when $w>w_c$. b is the width of the structure perpendicular to the plane and a_1 is the distance between nodes 1 and 2 (Fig. 48). The load F_2 is chosen so that $\sigma(1, 2)+ \sigma(2, 2)= f_t$ which means that, when load-case 1 and 2 are combined, the tensile strength is reached at node 2. The total load is then F_1+F_2 and the stresses at the different nodes are given as $\sigma(1, i)+ \sigma(2, i)$. The stresses at node 1 due to load F_2 is negative (the forces at this node want to widen the crack) and consequently the total stress at node 1 decreases according to the σ-w curve.

By using this method it is possible to choose the propagation direction of the fracture zone after each calculation step. Then the first principal stress is calculated at the tip of the fracture zone and propagation takes place along a path perpendicular to the first principal stress or, as the possible directions of propagation are limited to the directions of the element sides, along the element side which deviates less from the theoretical propagation direction.

4.6. Model of Zhou and Hillerborg

Zou and Hillerborg [101] proposed a time-dependent fracture model for concrete based on material tests. Under long-term loading, creep in the high stress zone around the fictitious crack tip may be high enough to reach the tensile strain capacity, so that crack formation can occur below the static tensile strength. Therefore the criterion should be adjusted for a time effect. Zou [100] used the static tensile strength as a criterion in all the models instead of using a stress-failure lifetime relation or stress-strain criterion.

Time dependent problems are often solved in increments by dividing time into small steps. Under sustained loading it is usual to evaluate incremental creep stains from stresses at the beginning of the time step and structural responses in the time increment can be obtained by imposing a pseudo load from the creep strains. Since this approach cannot be used in fracture zone Zhou performed a series of deformation-controlled tests on fracture zone. At the beginning of each time step, stress relaxations are computed instead, and consequently a pseudo load can be evaluated from the relaxation stresses. The time dependent σ-w relation is expressed in the following form:

$$d\sigma = d\sigma^{R} + d\sigma^{I} \tag{78}$$

where $d\sigma^{R}$ and $d\sigma^{I}$ are stress changes due to relaxation and the deformation increment dw respectively during the time increment dt.

Since it is quite difficult to perform relaxation tests during a long period of time, accurate stress-time functions in relaxation cannot be obtained from the tests. Therefore simple functions based on experimental evidences are proposed in the model to illustrate the main features of time effect in the fracture zone.

Fig. 50 illustrates the proposed model. During the time increment $dt = t_{i+1}$-t_i, the deformation is first held at w_i and the stress decrease $d\sigma^{R}$ due to relaxation is $\sigma_A - \sigma_i$. Then, when the deformation increases from w_i to w_{i+1}, the stress can increase until it reaches the envelop of the static σ-w curve at Point B along the path A-B and follow the curve until Point i+1. The stress change $d\sigma^{I}$ is $\sigma_{i+1} - \sigma_A$. Of course, if the deformation increment dw is small, then Point i+1 may not reach Point B and will instead locate at a point somewhere between A and B. The relaxation function of a modified Maxwell model is chosen.

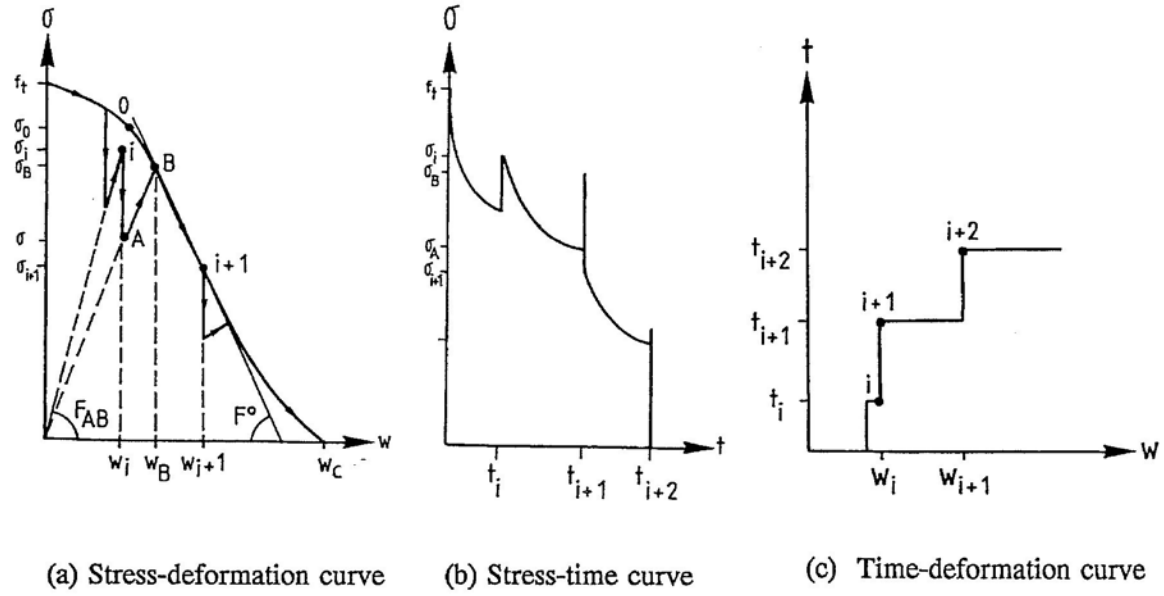

Fig. 50: Illustration of the model of Zhou [100]

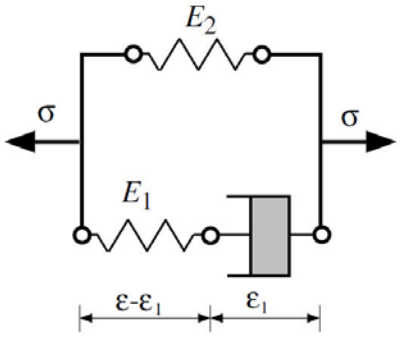

Fig. 51: Rheological model [103].

Zou and Hillerborg used a simple rheological element to illustrate the main features of the problems concerned. Rheology is concerned with time-dependent deformation of solids. In the simplest rheological model of the linear standard viscoelastic solid (Fig. 51), the springs are characterized by linear stress–displacement relationships:

$$\begin{aligned} \sigma_1 &= E_1(\varepsilon - \varepsilon_1) \\ \sigma_2 &= E_2\varepsilon \end{aligned} \tag{79}$$

The stress relaxation within time increment *dt* is assumed to be given by:

$$\begin{aligned} d\sigma^R &= (\sigma_i - \alpha\sigma_0)\left(\exp(-\frac{dt}{\tau}) - 1\right) && \sigma_i > \alpha\sigma_0 \\ d\sigma^R &= 0 && \sigma_i \le \alpha\sigma_0 \end{aligned} \tag{80}$$

where α is constant, σ_0 is the stress corresponding to w_i in the static σ-w relation and τ is relaxation time. The relaxation tests in tension show that stress relaxation seems to reach a limit value which is proposed to equal $\alpha\ \sigma_0$. Therefore, in the equation above the term $\alpha\ \sigma_0$ has been introduced as a relaxation limit. Stress relaxation below the limit is assumed to be zero.

The stress change $d\sigma^I$ is proposed as:

$$\begin{aligned} d\sigma^I &= F*(w_{i+1}-w_i) && w_{i+1}\le w_B \\ d\sigma^I &= F*(w_B-w_i)+F^0*(w_{i+1}-w_B) && w_{i+1}>w_B \end{aligned} \tag{81}$$

where,

$$\begin{aligned} F &= F_{AB}(\exp(-dt/\tau)+1)/2 \\ F_{AB} &= \frac{\sigma_A}{w_i}=\frac{\sigma_i+d\sigma^R}{w_i} \\ F^0 &= \frac{\partial\sigma^0}{\partial w}(w_B) \end{aligned} \tag{82}$$

and $\sigma^0(w)$ represents the static σ-w curve.

The experimental loading-reloading curve is complicated (Fig. 52), thus in the model a linear stiffness is proposed in the model to make a simple and proper description of the curve possible.

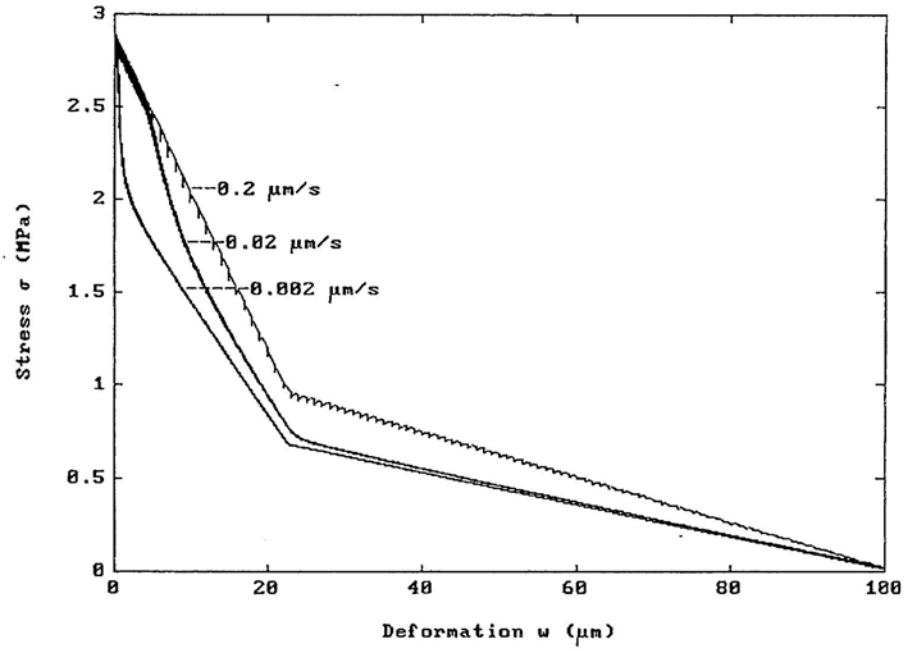

Fig. 52: Simulated tensile σ-w curves at different rates according to the model α=0.7, τ=25 second

In Fig. 52 the model is applied to simulate stress-deformation curves in different deformation rates. If the rate is high (close to static loading rate), the stress-deformation curve is near the static one. Meanwhile, the curve deviates more from the static one for slow rate, and the transmitting stress in the fracture zone becomes lower than the static one for the same deformation.

References

[1] ASCE-ACI Committee 426, The shear strength of reinforced concrete members, J Struct Div, ASCE 99 (6) (1973), pp. 1091–1187.

[2] Aster, H., Koch, R.,"Untersuchungen an dicken Stahlbetonplatten", Universität Stuttgart, 1974

[3] Walraven J.C., Fundamental analysis of aggregate interlock, J Struct Div, ASCE 108 (1981), pp. 2245–2270. View Record in Scopus | Cited By in Scopus (61)

[4] Walraven, J.C.,"The influence of depth on the shear strength of lightweight concrete beams without shear reinforcement", Report 5-78-4, Delft University of Technology, 1978.

[5] Mathey, R.G., Watstein, D. (1963), "Shear strength of beams without web reinforcement containing deformed bars of different yield strengths", ACI Journal Vol. 60., No. 2, Feb. 1963, pp183-207

[6] Leung, Y.W., Chew, C.B. and Regan, P.E. (1976), "Shear strength of various shapes of concrete beams without shear reinforcement", Polytechnic of Central London, 1976.

[7] Vecchio F.J. and M.P. Collins, The modified compression-field theory for reinforced concrete elements subjected to shear, ACI J 83 (2) (1986), pp. 219–231. View Record in Scopus | Cited By in Scopus (394)

[8] Loov R.E. and L. Peng, Shear strength of high strength concrete ACI 318-95 versus shear friction, ACI Special Publ SP-189 (1999), pp. 411–430.

[9] Vintzeleou E.N. and T.P. Tassios, Mathematical models for dowel action under monotonic conditions, Mag Concrete Res 38 (1986), pp. 13–22.

[10] Teller, L.W., Sutherland, E.C., The structural design of concrete pavements, Part 4, Public roads, vol. 17, no. 7/8, Sept./Oct. 1936, pp. 143-171/175-192.

[11] Timoshenko, S., Lessels, J.M., Applied elasticity, Westinghouse Technical Night School Press, East Pittsburgh, 1925, pp. 133-141.

[12] ASCE-ACI Committee 445, Recent approaches to shear design of structural concrete, J Struct Eng ASCE 124 (12) (1998), pp. 1375–1417.

[13] Talbot AN. Tests of reinforced concrete beams: resistance to web stresses series of 1907 and 1908. Bull. 29, University of Illinois Engineering Experiment Station, Urban, IL; 1909.

[14] Kani G.N.J., How safe are our large reinforced concrete beams, ACI J 64 (3) (1967), pp. 128–141.

[15] Swamy R.N., Adepegba D., 1969, Shear Resistance of Reinforced Beams without Web Steel, Building Science, Vol. 3, Issue 4, Feb. 1969, pp. 207-220

[16] Shioya T, Iguro M, Nojiri Y, Akiayma H, Okada T. Shear strength of large reinforced concrete beams, fracture mechanics: Application to concrete. ACI, 1989. SP-118, Detroit: p. 259–279.

[17] Bažant Z.P., Fracturing truss model: Size effect in shear failure of reinforced concrete, J Eng Mech, ASCE 123 (12) (1997), pp. 1276–1288. Full Text via CrossRef | View Record in Scopus | Cited By in Scopus (16)

[18] Collins, M.P., Evaluation of shear design procedures for concrete structures, A report prepared for the CSA Technical Committee on Reinforced Concrete Design, Canada, March 2001

[19] Kani G.N.J., The riddle of shear failure and its solution, ACI J 61 (2) (1964), pp. 441–467.

[20] Kani, G.N.J., Basic Facts Concerning Shear Failure- Part 1, ACI Journal, V. 63, No. 6, June 1966, pp675-692

[21] Kani, G.N.J., Basic Facts Concerning Shear Failure- Part 2, Supplement to Journal of ACI, ACI Publication, June 1966

[22] Zararis P.D., Shear compression failure in reinforced concrete deep beams, J Struct Eng ASCE 129 (4) (2003), pp. 544–553. Full Text via CrossRef | View Record in Scopus | Cited By in Scopus (6)

[23] Tureyen A.K. and R.J. Frosch, Discussion for Concrete shear strength: Another perspective, ACI Struct J 101 (4) (2004), pp. 582–587.

[24] Kim J. and Y. Park, Prediction of shear strength of reinforced concrete beams without web reinforcement, ACI Mater J 93 (3) (1996), pp. 213–222. View Record in Scopus | Cited By in Scopus (12)

[25] Brown MD. Design for shear in reinforced concrete using strut-and-tie and sectional models. Ph.D. dissertation. The University of Texas at Austin; 2005.

[26] Hegger J., A. Sherif and S. Görtz, Analysis of pre- and post-cracking shear behavior of prestressed concrete beams using innovative measuring techniques, ACI Struct J 101 (2) (2004), pp. 183–192. View Record in Scopus | Cited By in Scopus (5)

[27] Khuntia M., B. Stojadinovic and S.C. Goel, Shear strength of normal and high-strength fiber reinforced concrete beams without stirrups, ACI Struct J 96 (2) (1999), pp. 282–289. View Record in Scopus | Cited By in Scopus (22)

[28] EC2. Design of concrete structures Part I: General rules and rules for buildings. European Committee for Standardization. Brussels: 2002.

[29] ACI committee 318. Building code requirements for structural concrete (ACI 318-05) and Commentary (ACI 318R-05). USA. 2005.

[30] Eurocode 2 commentary, European Concrete Platform ASBL, June 2008

[31] Canadian standards association. CSA Technical committee on reinforced concrete design 2004. A23.3-04. Rexdale, Ontario. 2004.

[32] Regan, P.E. (1998),"Enhancement of shear resistance in short shear spans of reinforced concrete", an evaluation of UK recommendations and particularly of BD- 44/95, University of Westminster, London (14 pages).

[33] Choi K.K., A. G. Sherif, M. M. Reda Taha, L. Chung, Shear strength of slender reinforced concrete beams without web reinforcement: A model using fuzzy set theory, J Engineering Structures (31) (2009), pp768-777

[34] Hedman, O., Losberg, A. (1978), "Design of concrete structures with regard to shear forces", CEB Bulletin d'Information No. 126, pp. 184-209.

[35] Junga S. and K. S. Kim, Knowledge-based prediction of shear strength of concrete beams without shear reinforcement, J Engineering Structures (30) (6), June 2008, pp1515-1525

[36] Fenwick, R.C. and Paulay, T. (1968), Mechanisms of Shear Resistance of Concrete Beams, *Journal of the Structural Division*, ASCE, Vol. 94, No. ST10, pp. 2235-2350

[37] MacGregor, J.G. (1988), Reinforced Concrete: Mechanics and Design, Prentice Hall, Englewood Cliffs, New Jersey.

[38] Leonhardt, F. (1978), "Shear in Concrete Structures", CEB Bulletin d' Information No 126: Shear and Torsion, pp. 66-124

[39] Taylor, H.P.J. (1972), Shear Strength of Large Beams", Journal of the Structural Division, Vol. 98, No. 11, pp. 2473-2490

[40] Taylor, H.P.J. (1970), The Fundamental Behaviour of Reinforced Concrete Beams in Bending and Shear, *Shear in Reinforced Concrete*, ACI SP-42, paper 3, pp. 43-77

[41] Hamadi Y. D. and Regan P. E. Behaviour in shear of beams with flexural cracks. *Magazine of Concrete Research*, 1980, 32, No.111, pp. 67–78

[42] Joint ACI-ASCE Committee 445, (1998), Recent Approaches to Shear Design of Structural Concrete, *Journal of Structural Engineering*, ASCE,V. 124, No. 12, Dec., pp. 1375-1417.

[43] Hillerborg A., Modéer M. and Peterson P.E. (1976), Analysis of crack formation and crack growth in concrete by means of fracture mechanics and finite elements, *Cement Concrete Res*. Vol. 6, pp. 773–782.

[44] Bažant, Z.P., and Oh, B.-H. (1983). "Spacing of cracks in reinforced concrete." J. of Structural Engineer- ing, ASCE, 109, 2066–2085.

[45] Rafla K., Empirical Formula for the Design on Shear Force Resistance of concrete Beams, 1971

[46] Regan, P.E. (2000), Aspects of diagonal tension in reinforced concrete, Structural Concrete, Journal of fib, No. 13, Sep. 2000, pp119-132

[47] König, G.; Fischer, J.: Model Uncertainties concerning Design Equations for the Shear Capacity of Concrete Members without Shear Reinforcement, Comité European du Beton (CEB), Bulletin N° 224, Lausanne, 1995

[48] Hedman, O., Losberg, A.: Design of Concrete Structures with Regard to Shear Forces, CEB Bulletin 126, PP. 184-209d, Paris, 1978

[49] Nielsen, M.P. (1990), "Commentaries on Shear and Torsion", Eurocode 2 editorial Group – 1st draft – October 1990.

[50] Hognestadt, E. ,Elstner, R.C. (1957), "Laboratory investigation of rigid frame failure", ACI Journal, V.53 No. 1, Jan 1957, pp. 637-668.

[51] Pruijssers A.F., Shear resistance of beams based on the effective shear depth, University of Technology Report No.5-86-1, Delft

[52] Regan, P.E. (1971), "Shear in reinforced concrete – an experimental study", Technical Note 45, CIRIA, London.

[53] Regan, P.E. (1999), "Ultimate Limit State Principles: Basic design for moment, shear and torsion", in fib Text Book on Structural Concrete, Vol. 2, pp. 141-223.

[54] Leonhardt F. and Walther, Contribution to the Treatment of Shear Problems in Reinforced Concrete (Beiträge zur Behandlung der Schubprobleme in Stahlbetonbau), Beton-und Stahlbetonbau (Berlin), V. 56, No 12, Dec. 1961

[55] Bažant Z.P. and S. Prasannan, (1989). "Solidification theory for concrete creep. I: Formulation II: Verification and application." J. Engng. Mech., ASCE, 115(8), pp1691-1725

[56] Comité Euro-International du Béton: Evaluation of the Time Dependent Behaviour of Concrete. Bulletin D'Information No. 199, Lausanne, 1990

[57] Comité Euro-International du Béton: CEB-FIP Model Code 1990 (CEB_FIP MC90). Bulletin D'Information No. 213/214, Lausanne, May 1993

[58] ENV 197-1 Cement – Composition, production, placing and compliance criteria – Part 1: Common cements, 1992

[59] Comité Euro-International du Béton: FIB Bulletin 1: Structural Concrete – Textbook on behaviour, design and performance. Vol. 1, July 1999

[60] Awad M.E. and H.K. Hilsdorf: Strength and deformation characteristics of plain concrete subjected to high repeated and sustained stresses. Abeles Symposium on Fatigue of Concrete, American Concrete Institute, SP-41, 1974, pp1-13

[61] Regan, P.E., Al-Hussaini, A., Ramdane K-E., Xue H-Y., (1993). "Behaviour of High Strength Concrete Slabs", Concrete 2000. Proceedings of International Conference, University of Dundee, Scotland, UK, September 7-9, Vol. 1, E&FN Spon, Cambridge, pp. 761-773.

[62] Rüsch H., Researches Toward a General Flexural Theory for Structural Concrete. Journal, American Concrete Institute, Vol. 32, July 1960, pp1-28

[63] Paulay T. and Loeber P. (1974), Shear transfer by aggregate interlock, American Concrete Institute, Special Publication SP 42–1, pp. 1–15.

[64] Taerwe, L.,Towards a consistent treatment of model uncertainties in reliability formats for concrete structures, CEB Bulletin 219, 1993, pp5-61

[65] Bažant Z.P, Mathematical Modelling of Creep and Shrinkage of Concrete, John Wiley & Sons Ltd. Chchester, 1988

[66] Kotsovos M. D., and Pavlović M., Ultimate limit-state design of concrete structures: a new approach, Thomas Telford, London, 1999

[67] Cladera Bohigas, A., Shear design of reinforced high-strength concrete beams, PhD Thesis, Universitat Politëcnica de Catalunya, Barcelona, December 2002

[68] Rüsch H., D. Jungwirth and H.K. Hilsdorf: Creep and Shrinkage – Their Effect on the Behaviour of Concrete Structures. Springer Verlag Newyork, Heidelberg, Berlin, 1983

[69] Scordelis A.C., Nilson A.H., Grestle K. (1982), Finite Element Analysis of Reinforced Concrete, ASCE State-of-the-Art Report, New York

[70] Gambarova, P.G. (1987), “Modelling of interface problems in reinf. Concrete”, Proc. IABSE coll.,. Computational mech. of concrete struct., Delft, Aug. 1987, pp. 1-16.

[71] Baźant , Z. P., and Gambarova, P. (1980), "Rough Cracks in Reinforced Concrete,". Journal of the Structural Division, ASCE, Vol. 106, No. ST4, April 1980, pp. 819-842.

[72] Baźant , Z.P., Gambarova, P. (1984), "Crack shear in concrete: Crack band micro plane model." J. Struct. Eng., ASCE, 110, pp.2015-2036.

[73] Dei Poli, S., Gambarova, P.G., Karakoč: Aggregate interlock role in reinforced concrete thin-webbed beams in shear, J. of struct, eng., ASCE, vol.

[74] Walraven, J.C. (1980), Aggregate interlock: a theoretical and experimental analysis, Ph.D. Thesis, Delft Institute of Technology, Delft, 1980, 197 pp.

[75] Walraven J.C. and Reinhardt H.W. (1981), Theory and experiments on the mechanical behaviour of cracks in plain and reinforced concrete subjected to shear loading, Heron, vol. 26, No 1a, 68 pp.

[76] Walraven J C, Keuser W. (1987), "The shear retention factor as a compromise between numerical simplicityand realistic material behavior". Darmstadt Concrete. 2. pp. 221-234.

[77] Frenaij J. W. I. J., J. C. Walraven, and H. W. Reinhardt, Time-dependent shear transfer in cracked reinforced concrete, 1988, Delft

[78] Eurocode 2. Design of concrete structures. General rules, BS EN 1992-1:2004

[79] Walraven, J.C., Lehwalther, N. (1994), “Size effects in short beams loaded in shear”, *ACI - Structural Journal*, Vol. 91, No. 5., Sept.-Oct. 1994, pp. 585-593.

[80] Wittmann, F.H. and Zaitsev, J. (1974), "Verformung and Bruchvorgang poröser Baustoffe bei kurzzeitiger Belastung und Dauerlast", Schtiftenreihe Deutscher Ausschuß für Stahlbeton, Heft 232.

[81] Vecchio, F. J., and Collins, M. P. “The Modified Compression Field Theory for Reinforced Concrete Elements Subjected to Shear,” ACI JOURNAL, Proceedings V. 83, No. 2, Mar.-Apr. 1986, pp. 219-231.

[82] Moody, K.G., Viest, M., Elstner, R.C. and Hognestad, E. (1954), “Shear Strength of Reinforced Concrete Beams-Part 1: Tests of Simple Beams,” *ACI JOURNAL, Proceedings* V. 51, No. 4, Apr. 1954, pp. 317-332.

[83] Muttoni A. and Fernández Ruiz M. (2008), “Shear Strength of Members without Transverse Reinforcement as Function of Critical Shear Crack Width”, *ACI STRUCTURAL JOURNAL*, March-April, 2008.

[84] Jenq, Y.S. and Shah, S.P. (1988), “Mixed Mode Fracture of Concrete”, *International Journal of Fracture*, Vol. 38, pp. 123-142.

[85] Taha, N.M. and Swartz, S.E. (1989), “Crack Propagation Models for Mixed-Mode Loading”, *Fracture of Concrete and Rock,* S.P. Shah, S.E. Swartz and B. Barr, Eds., 1989, PP. 5-17.

[86] Ballatore, E., Carpinteri, A., Ferrara, G. and Melchiorri, G. (1990), Mixed Mode Fracture Energy of Concrete”, *Engineering Fracture Mechanics*, Vol. 35, No. 1/2/3, pp. 145-157.

[87] Xu, S. and Reinhardt, H.W. (2005), “Shear Fracture on the Basis of Fracture Mechanics”, *Otto-Graf-Journal*, Vol. 16, pp. 21-78.

[88] Erdogan, F. and Sih, G. C. (1963), “On the crack extension in plates under plane loading and transverse shear”, *J. Basic Engng*, *ASME*, Vol 85, pp. 519-527.

[89] Sih, G.C. (1974), “Strain energy density factor applied to mixed mode crack problems”, *Int. J. Fracture*, Vol 10, pp. 305-321.

[90] Hussain, M. A., Pu, S. L. and Underwood, J. (1974), “Strain-energy release rate for a crack under combined mode I and mode II”, *ASTM* STP 560, pp. 2-28.

[91] Buyukozturk, O. and Lee, K.M. (1992), “Mixed Mode Fracture Concepts in Structural Design”, *Special. Publication Series of American Concrete Institute (ACI)*, SP-134, pp. 47-62.

[92] Kaplan, M.F. (1961), Crack propagation and the fracture of concrete. *Journal of the American Concrete Institute*, Vol. 58, pp. 591-609.

[93] PETERSSON. P. E. Fracture energy of concrete: method of determination. Cement and Concrete ResearchV. ol. IO, No. 1, 1980. pp. 78-89. (Ref. 7 of original paper.)

[94] GRIFFITH AA, The phenomena of rupture and flow in solids. Philosophical Transactions of the Royal Society of London, Sereis A, 221:163-198, 1921.

[95] Barenblatt G. (1962), The mathematical theory of equilibrium crack in the brittle fracture. *Advanced in Applied Mechanics*, Vol. 7, pp. 55–125

[96] Dugdale D.S. (1960), Yielding of steel sheets containing slits. *J. of Mech. Phys. Solids*, Vol. 8, pp. 100-104

[97] Atrushi D.S. (2003), Tensile and Compressive Creep of Early Age Concrete: Testing and Modelling, Doctoral Thesis, The Norwegian University of Science and Technology, Trondheim, Norway, 314 pp.

[98] Šerda, Z. and Křístek, V. (1988): "Creep and Shrinkage of Concrete Elements and Structures". Developments in Civil Engineering, 21, Czechoslovakia.

[99] Morsch, E. (1902), Der Eisenbetonbau, seine Anwendung und Theorie. *Neustadt A. D. Haardt: Wayss and Freytag*, Stuttgart.

[100] Zhou, F.P. (1992), Time-dependent crack growth and fracture in concrete. PhD thesis, Report TVBM-1011, Lund University of Technology, Sweden.

[101] Zhou, F.P., Hillerborg, A. (1992), Time-dependent fracture of concrete: testing and modelling. In: Ba zant, Z.P. (Ed.), Fracture Mechanics of Concrete Structures. Elsevier Applied Science, The Netherlands, pp. 906–911.

[102] Illston, J. M. (1965), The creep of concrete under uniaxial tension, Magazine of Concrete Research, Vol.17, No.51, June 1965, pp.77-84.

[103] Barpi F. and Valente S. (2004), A fractional order rate approach for modeling concrete structures subjected to creep and fracture, *International Journal of Solids and Structures*, Vol. 41, pp. 2607–2621

[104] Čerepanov G. P. (1968), Cracks in Solids, *Int. Journ. Solids and Structures*, Vol. 4, pp.811.